ACS NANO

Open Access

www.acsnano.org

ARTICLE

Production of Plant Virus-Derived Hybrid Nanoparticles Decorated with Different Nanobodies

Enrique Lozano-Sanchez, José-Antonio Daròs,* and Fernando Merwaiss*

Cite This: *ACS Nano* 2024, 18, 33890−33906

Read Online

ACCESS | Metrics & More | Article Recommendations | Supporting Information

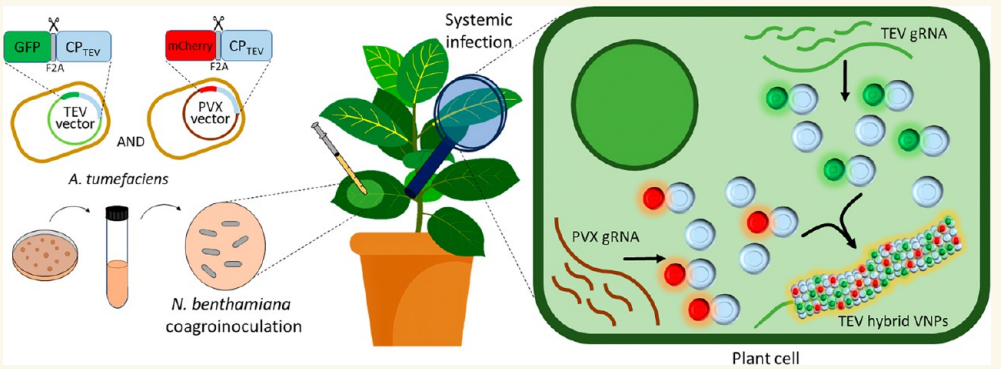

ABSTRACT: **Viral nanoparticles (VNPs) are self-assembled nanometric complexes whose size and shape are similar to those of the virus from which they are derived. VNPs are arousing great attention due to potential biotechnological applications in fields like nanomedicine and nanotechnology because they allow the presentation of polypeptides of choice linked to the virus structural proteins. Starting from tobacco etch virus (TEV), a plant plus-strand RNA virus that belongs to the genus *Potyvirus* (family *Potyviridae*), here we describe the development of recombinant hybrid VNPs in *Nicotiana benthamiana* plants able of exposing simultaneously different proteins on their surface. This system is based on the synergic coinfection of TEV and potato virus X (PVX; *Potexvirus*), in which PVX provides a second TEV CP *in trans* allowing a mixed assembly. We first generated genetically modified hybrid VNPs simultaneously displaying green and red fluorescent proteins on their surface. A population of decorated and nondecorated CPs resulting from the insertion of the picornavirus F2A ribosomal escape peptide was required for viral particle assembly. Correct assembly of the recombinant mosaic VNPs presenting the exogenous peptides was successfully observed by immunoelectron microscopy. We next achieved the production of hybrid VNPs expressing a nanobody against SARS-CoV-2 and a fluorescent reporter protein, whose functionality was demonstrated by ELISA and dot-blot assay. Finally, we engineered the production of hybrid multivalent VNPs carrying two different nanobodies against distinct epitopes of the same SARS-CoV-2 antigenic protein, emulating a nanobody cocktail. These plant-produced recombinant mosaic VNPs, which are filamentous and flexuous in shape, presenting two different fused proteins on the surface, represent a molecular tool with several potential applications in biotechnology.**

KEYWORDS: *hybrid viral nanoparticle, plant virus, molecular farming, nanobody, tobacco etch virus, potato virus X*

INTRODUCTION

Viral nanoparticles (VNPs) are virus-based assemblies potentially useful in nanotechnology and nanomedicine, in applications such as antigen presentation, drug delivery and targeted bioimaging.[1−4] VNPs are attracting interest due to their exceptional structural features and easy functionalization. Advantages of VNPs comprise self-assembly with specific stoichiometry, remarkable stability, biocompatibility, and easy

Received: May 28, 2024
Revised: November 6, 2024
Accepted: November 18, 2024
Published: December 2, 2024

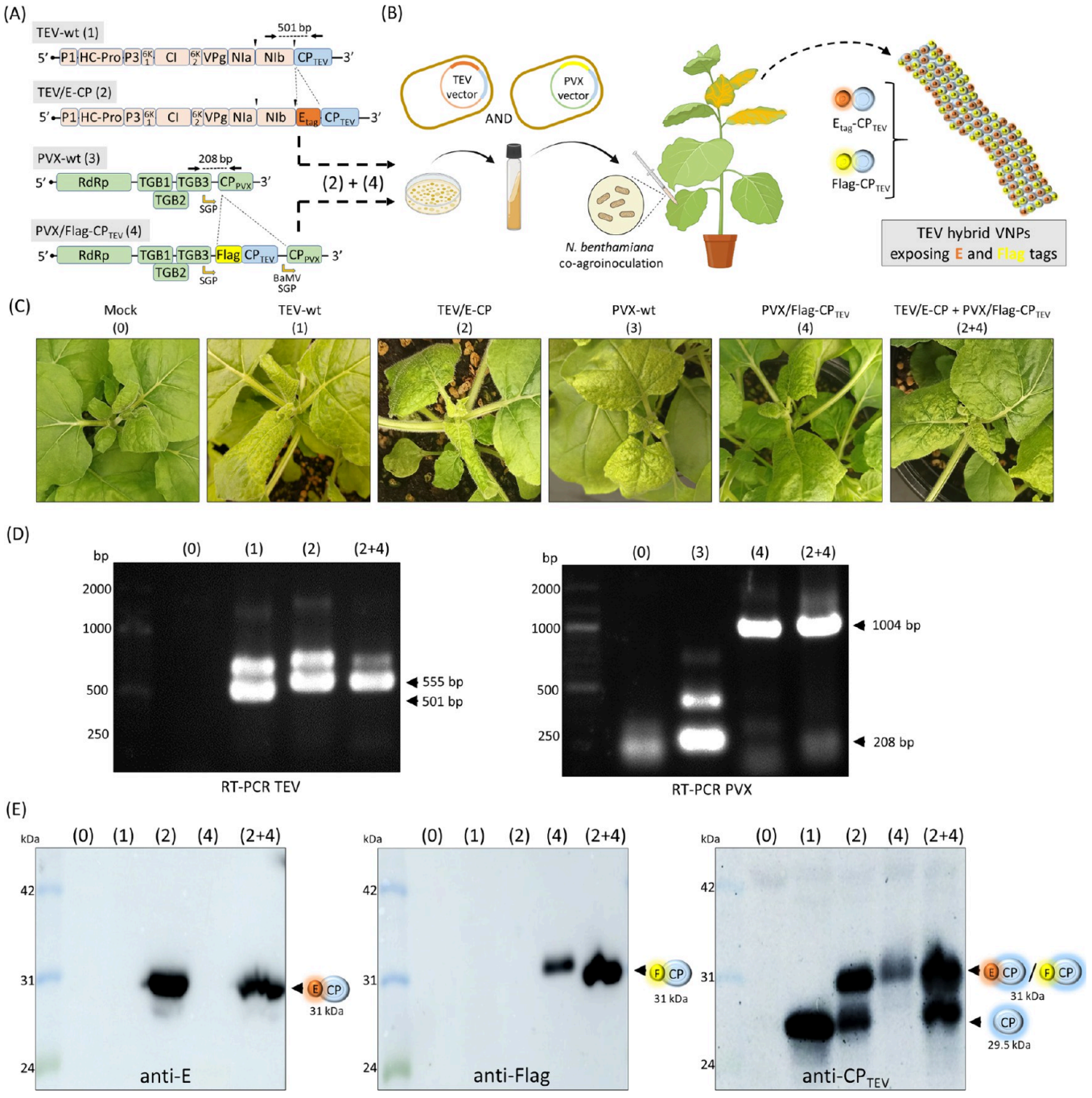

Figure 1. Production of TEV-derived hybrid VNPs carrying a mixture of modified CPs by coinfection with a PVX vector. (A) The E tag was cloned fused to the amino terminal end of CP_{TEV} maintaining the native processing sites of the polyprotein in the TEV infectious clone (constructs 1 and 2). The CP_{TEV} sequence fused to a Flag tag was cloned in the PVX vector under the endogenous CP subgenomic promoter of the PVX infectious clone (constructs 3 and 4). (B) *A. tumefaciens* was transformed with TEV or PVX recombinant vectors and used to coagroinoculate *N. benthamiana* plants. Cells coinfected with both viral vectors expressed both CP-fused proteins, potentially allowing the assembling of hybrid VNPs. (C) Representative pictures at 10 dpi of the upper leaves of plants mock-inoculated (0), inoculated with all the individual viral clones (1, 2, 3 and 4) and coagroinoculated with clones 2 and 4. (D) The presence of both recombinant viruses in the corresponding symptomatic upper leaves was analyzed by RT-PCR with primers flanking the insertion sites (shown in A). Amplification products were separated via electrophoresis in agarose gels (RT-PCR for TEV on the left and RT-PCR for PVX on the right). (E) The expression of both peptide-fused CPs (E-CP and Flag-CP) was detected by Western blot with the corresponding conjugated antibodies against the fused peptides (left and middle panels, respectively) and against the CP_{TEV} (right panel). The positions and sizes of the protein standards are indicated on the left. Black arrows indicate the positions of the respective proteins.

biodegradation. Engineering the viral genome is the easiest strategy to display small polypeptides, and viral coat protein (CP) represents the perfect scaffold to fuse foreign molecules of interest.[5−7]

Molecular farming is a biotechnological field that refers to the recombinant generation of biotechnologically useful products in plants. Several studies have demonstrated the ability of plants to produce valuable proteins, including a growing amount of those

https://doi.org/10.1021/acsnano.4c07066
ACS Nano 2024, 18, 33890−33906

entering clinical trials, and some even reaching the market as approved biologics.[8−11] This manufacturing process, typically using *Nicotiana benthamiana* plants as biofactories, has shown great potential for expressing proteins due to short development times and lower regulatory burden.[12,13] In particular, the use of viruses as vectors for expression in plants has been extensively characterized in biotechnology, particularly to produce heterologous proteins.[14] Moreover, plant-virus-based VNPs, with different morphologies, have satisfactorily been converted into scaffolds for the presentation of polypeptides of interest that can be either encoded in the viral genome or conjugated chemically to the surface proteins of the virions. Aiming to develop diagnostic reagents or recombinant vaccines, researchers have mostly concentrated on VNPs harboring antigenic epitopes belonging to pathogens.[15−17] Following this approach, the immune response to antigens with low immunogenicity is improved due to the inherent capability of VNP to elicit immunity. Some of the plant viruses frequently employed in this field include cowpea mosaic virus (CPMV),[18−20] tobacco mosaic virus (TMV)[21,22] or potato virus X (PVX), representing icosahedral, rod and flexuous morphologies, respectively. However, less-explored viruses that might carry larger transgene cargoes and improve the host range are being studied.[15]

Tobacco etch virus (TEV) belongs to the genus *Potyvirus* within the family *Potyviridae*. TEV consists of ca. 750 nm-long filamentous flexuous virions that encapsidate a genomic RNA molecule of about 9500 nt. Several features make potyviruses appealing as VNP scaffolds. The elongated shape of the viral particles permits insertion of larger foreign genetic cargoes, while the larger surface area of this kind of particles results in additional positions for functionalization in comparison with other virion morphologies.[23−25] In fact, some potyviruses have been employed as scaffolds for antigen display, resulting in higher immunogenicity.[26−29] Potyviruses have been successfully applied as antigen presentation scaffolds either by expressing chimeric CPs using heterologous systems to produce VLPs or by infecting host plants with recombinant viruses with CP-fused foreign peptides.[30]

We have recently demonstrated the use of potyviruses for the production of genetically encoded VNPs carrying nanobodies (VHH, variable heavy chain) against the Spike (receptor binding domain, RBD) of the severe acute respiratory syndrome coronavirus 2 (SARS-CoV-2).[31,32] Moreover, these VNPs were able to completely neutralize pseudovirus infection in cell culture assays, and the neutralizing activity was increased compared to a recombinant antibody consisting of a divalent VHH domain. Here, we go a step further with the development of recombinant hybrid VNPs derived from TEV, in which more than one molecule of interest is exposed on their surface. This system is based on TEV and PVX infectious synergism,[33,34] in which this latter virus provides a second TEV CP (CP_{TEV}) *in trans* allowing a mixed assembly.

As a first approach, we generated genetically modified TEV-derived VNPs copresenting two different fluorescent proteins, green (GFP) and red (mCherry), on their surface. A mixed population of labeled and unmodified CP_{TEV} resulting from the addition of picornavirus ribosomal escape peptide F2A was needed to allow the assembly of the viral particles. The correct morphology of the recombinant mosaic VNPs presenting the exogenous peptides was successfully observed by immunoelectron microscopy. We next produced hybrid VNPs decorated with a nanobody against SARS-CoV-2 and a fluorescent reporter protein, the functionality of which was demonstrated by enzyme-linked immunosorbent assay (ELISA) and dot-blot. Finally, we engineered hybrid multivalent VNPs carrying two different nanobodies against distinct epitopes of the same antigenic SARS-CoV-2 protein, emulating a nanobody cocktail. These plant-produced recombinant TEV-derived nanoparticles, presenting simultaneously different recombinant proteins on the surface, may find biotechnological applicability in nanotechnology and nanomedicine.

RESULTS

Production of TEV-Derived Hybrid VNPs by Coinfection with a PVX Vector. We have recently reported on the use of TEV-based VNPs as scaffolds for peptide display using a gene-encoding strategy.[32] This technology relies on cloning the sequence of interest fused to the amino terminal end of the viral CP. Once expressed in the infected plant cells, the modified CPs are able to assemble, forming the recombinant VNPs, without hindering the viral replication or systemic movement. In this work, we aimed to move further, focusing on the production of hybrid VNPs by the coexpression of differently modified CPs in the same host cells. For this goal, we took advantage of the reported synergistic infectivity of plant viruses belonging to the genera *Potexvirus* and *Potyvirus*.[33,34] In particular, we envisioned a coinfection system in which a PVX-derived vector expresses a modified CP_{TEV} *in trans*, which could be assembled together with the CP_{TEV} produced by TEV *in cis*.

To set up this system, we designed a proof-of-concept assay in which the E tag epitope was cloned and fused to the CP amino-terminal end in the TEV genome. The recombinant clone (TEV/E-CP) maintained the native processing sites of the polyprotein. An additional CP_{TEV} sequence was then cloned in a PVX vector under its endogenous CP subgenomic promoter and fused to a Flag epitope, also at its amino-terminal end (PVX/Flag-CP_{TEV}). PVX CP was expressed from a heterologous promoter (Figure 1A). This second CP_{TEV} sequence was codon-optimized for *N. benthamiana* expression in order to avoid the presence of sequence repetitions between both viral genomes. We expected that following systemic infection of the plant with both recombinant viruses, TEV chimeric virions would be assembled in the upper leaves (Figure 1B). With this aim, *Agrobacterium tumefaciens* were transformed with plasmids containing both recombinant viruses, and *N. benthamiana* plants were single or coagroinoculated. Control plants were also agroinoculated with wild-type viruses as well as mock-inoculated. At 10 days postinoculation (dpi), all plants, but the mock-inoculated controls, showed symptoms of infection on the upper leaves, suggesting the unaltered systemic infection capacity of both recombinant viruses. Representative pictures are shown in Figure 1C. To confirm the presence of the corresponding recombinant viruses in the symptomatic upper leaves, we used reverse transcription (RT) followed by polymerase chain reaction (PCR) with primers flanking the insertion sites. Amplification products were separated via electrophoresis in agarose gels (Figure 1D). As expected, no amplification products were obtained in the mock-inoculated plants, while the plants inoculated with wild-type TEV (TEV-wt) and PVX (PVX-wt) showed the expected products of 501 and 208 base pairs (bp), respectively. The plants agroinoculated with TEV/E-CP produced a band of 555 bp, while those agroinoculated with PVX/Flag-CP_{TEV} showed a band of 1004 bp, in agreement with CP_{TEV} modification. Finally, the plant coagroinoculated with both recombinant viruses produced 555

https://doi.org/10.1021/acsnano.4c07066
ACS Nano 2024, 18, 33890−33906

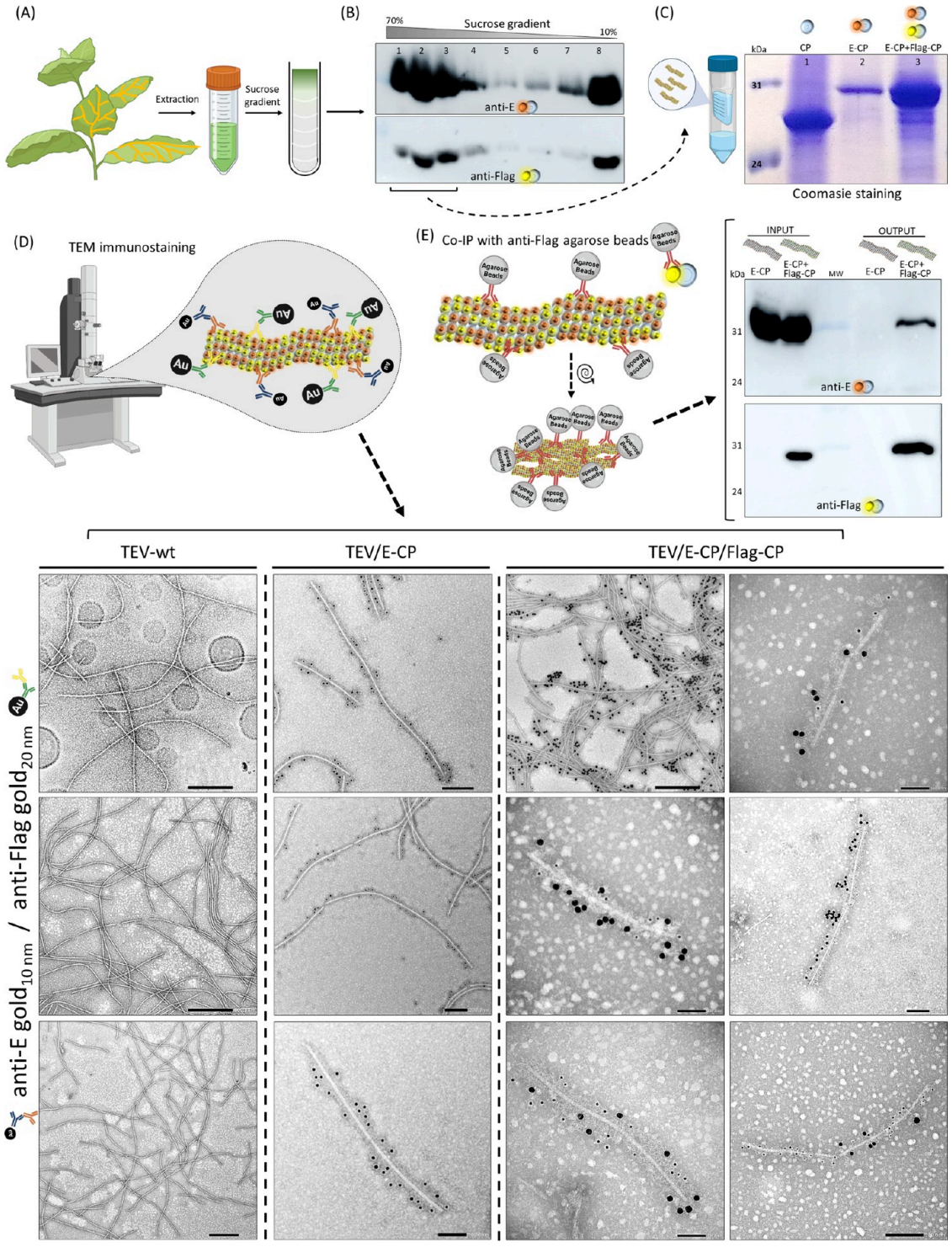

Figure 2. Purification and analysis of hybrid VNPs. (A) Symptomatic tissues were harvested at 10 dpi and homogenized in extraction buffer. VNPs were purified by several ultracentrifugation steps, including a sucrose gradient. (B) Gradient fractions were analyzed by Western blot against the two different CP-fused tags, and positive fractions for the presence of both recombinant CPs were pooled, dialyzed, and concentrated. (C) The product was analyzed by SDS-PAGE with Coomassie brilliant blue staining. Lane 1, TEV-wt; lane 2, TEV/E-CP; and lane 3, TEV/E-CP/Flag-CP. (D) Analysis of assembled hybrid VNPs carrying two different fused-CPs by TEM coimmunostaining. E-CPs and Flag-CPs were detected with antibodies conjugated to 10 and 20 nm gold spheres, respectively. Representative TEM images of the coimmunostaining of the TEV-wt (left column), TEV/E-CP (second column), and TEV hybrid VNPs (third and fourth columns). (E) The presence of both fused-CPs in assembled hybrid VNPs was also demonstrated by coimmunoprecipitation. Hybrid VNPs were pulled-down with anti-Flag coated agar beads. TEV/E-CP VNPs were used as a negative control. The co-IP input and output were analyzed by Western blot with anti-E or anti-Flag antibodies.

and 1004-bp bands in both analyses, confirming the successful systemic coinfection of both recombinant viruses.

Next, we analyzed the expression of the corresponding recombinant CPs. To this purpose, we used polyacrylamide gel

https://doi.org/10.1021/acsnano.4c07066
ACS Nano 2024, 18, 33890−33906

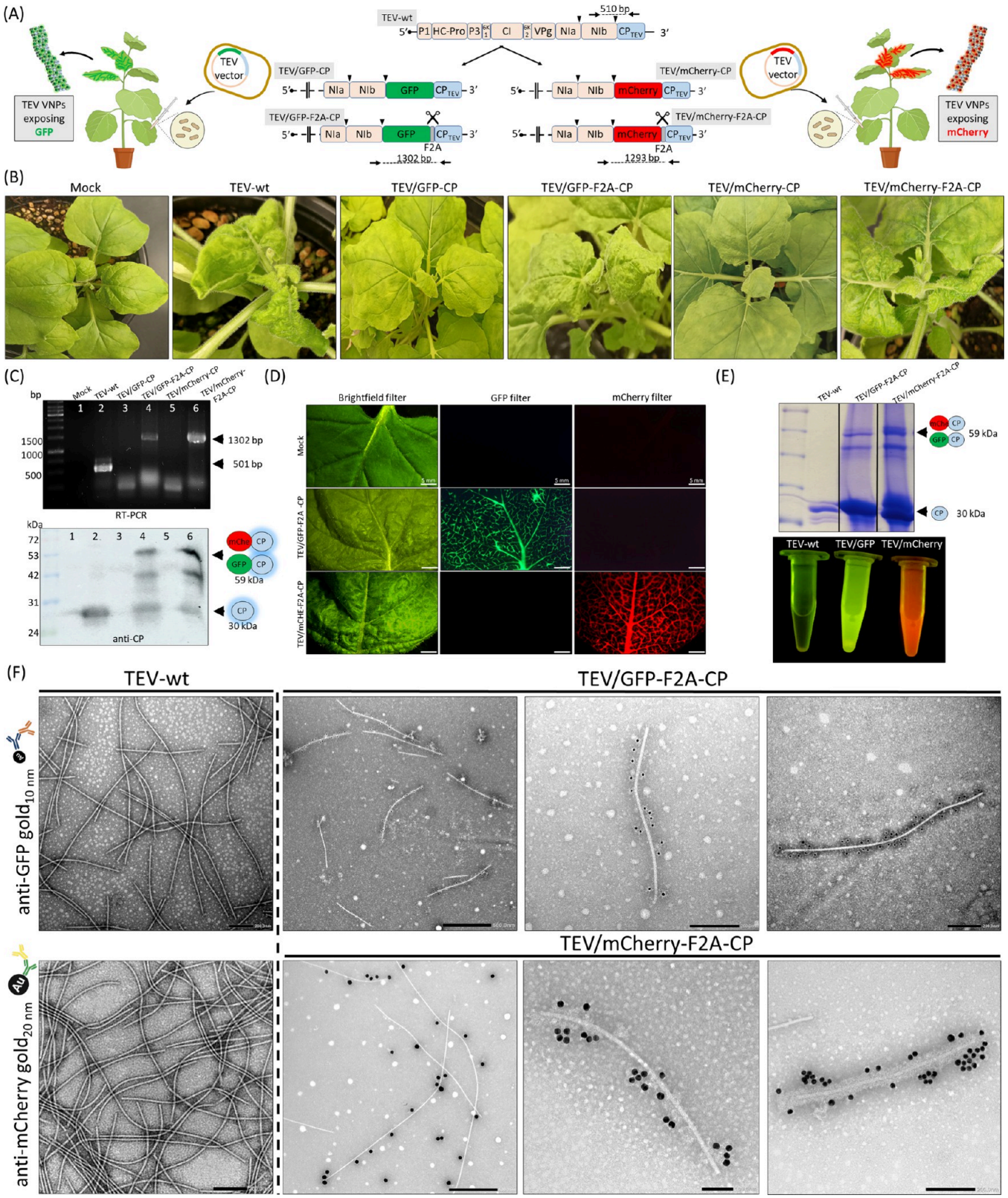

Figure 3. Production of TEV derived VNPs decorated with fluorescent proteins. (A) GFP and mCherry cDNAs were cloned fused to the viral CP with or without the F2A splicing peptide in between, maintaining the native polyprotein processing sites. (B) Pictures of representative upper leaves from *N. benthamiana* plants agroinoculated with all the different constructs, including TEV-wt and mock-inoculated controls, at 14 dpi. (C) Plant tissues were collected at 14 dpi and the presence of recombinant TEV progeny was analyzed by RT-PCR (top) with primers flanking the insertion site (shown in A) and by Western blot using an antibody against CP_{TEV} (bottom). Lanes 1, mock-inoculated plant; lanes 2 to 6, plants agroinoculated with TEV-wt, TEV/GFP-CP, TEV/GFP-F2A-CP, TEV/mCherry-CP and TEV/mCherry-F2A-CP, respectively. The positions and sizes of DNA and protein standards are indicated on the left. Black arrowheads indicate the positions of the CP_{TEV} fusion and free CP_{TEV}. (D) Stereomicroscope pictures of infected *N. benthamiana* leaves under visible light, green fluorescence, and red fluorescence

https://doi.org/10.1021/acsnano.4c07066
ACS Nano 2024, 18, 33890−33906

Figure 3. continued

conditions. Bar: 5 mm. (E) VNPs were purified as previously described and the purification product was analyzed by SDS-PAGE and Coomassie brilliant blue staining (top) and its fluorescence visualized under UV light (bottom). Black arrows indicate the positions of the CP_{TEV} fused protein and free CP_{TEV}. (F) Purified recombinant VNPs were analyzed by TEM and the presence of GFP or mCherry presented on their surfaces was detected by IEM. GFP was detected with a primary anti-GFP and a secondary anti-mouse conjugated to 10 nm gold particles. mCherry was detected with a primary anti-mCherry and a secondary anti-rabbit antibody conjugated to 20 nm gold spheres. Three different images are shown for each VNP purification. Images of a TEV-wt negative control are also included on the left.

electrophoresis (PAGE), with denaturing gels that contained sodium dodecyl sulfate (SDS; SDS-PAGE), to analyze samples collected from different agroinoculated plants. Three different Western blots were performed, and each of them was revealed with a different antibody. The presence of the CP expressed *in cis* by the TEV vector was detected with an anti-E antibody while the expression of the CP_{TEV} produced *in trans* by the PVX vector was detected with an anti-Flag antibody (Figure 1E, left and center). Lastly, the presence of both recombinant CPs was also confirmed by simultaneous detection using an anti-CP_{TEV} antibody (Figure 1E, right).

Subsequently, we sought to analyze the correct assembly and chimeric identity of the recombinant VNPs. Centrifugation in a sucrose gradient was used to fractionate extracts obtained from infected tissues (Figure 2A). Fractions analyzed by Western blot using both anti-E or anti-Flag antibodies showed efficient separation of the free CP monomers (i.e., not assembled) on the light gradient fractions and the coexistence of presumably assembled chimeric VNPs in the fractions corresponding to the heavy part of the gradient (Figure 2B). All the fractions with VNPs were mixed and subjected to dialysis and centrifugal concentration employing filter devices. TEV-wt and recombinant TEV/E-CP were also purified from infected tissues as controls. Finally, purified VNPs were analyzed by SDS-PAGE and gels were stained with Coomassie brilliant blue. We detected wild-type TEV CP (29.5 kDa), the larger E-CP derivative (31 kDa) and the mix of both derivative species (E-CP and Flag-CP) in the corresponding plants. The different CP species were detected by Western blotting employing the antibodies indicated above (Figure 2C). Next, we used coimmunoelectron microscopy (co-IEM) to analyze if the purified recombinant VNPs were correctly assembled and showed a chimeric display of both recombinant CPs. For this analysis, we performed an immunostaining using a mix of two primary antibodies (anti-E and anti-Flag) followed by a mix of two secondary antibodies (anti-mouse and anti-rabbit) conjugated to gold 10 or 20 nm spheres, respectively. Images of the TEV-wt negative control are depicted in Figure 2D (left column) showing no unspecific signal, while three representative images of TEV/E-CP (second column) showed staining exclusively with the 10 nm gold spheres, as expected. Conversely, the 6 representative images from the hybrid VNPs (third and fourth columns) showed the presence of gold spheres of both sizes attached to the same particles. These images showed the characteristic TEV filamentous virions homogeneously decorated with both types of gold spheres, which supported the successful generation of hybrid chimeric VNPs.

To further confirm these results, the presence of both fused-CPs in assembled hybrid VNPs was also proved by coimmunoprecipitation. Hybrid VNPs were pulled-down with anti-Flag coated agar beads, while TEV/E-CP VNPs were employed as a negative control. Western blot of the coimmunoprecipitation input and output showed that E-CPs were specifically pulled down when they were expressed along the Flag-CPs, supporting the assembly of hybrid VNPs (Figure 2E, top). The same samples were analyzed with an anti-Flag antibody as a control of the presence of this type of modified CPs only in the corresponding sample (Figure 2E, bottom). These experiments demonstrate the generation of TEV-based hybrid VNPs containing two different foreign peptides in *N. benthamiana* plants using a synergistic coinfection system.

Production of TEV Derived VNPs Decorated with Fluorescent Proteins. After proving the production of hybrid VNPs in which small tags were fused to different CPs, we intended to produce hybrid VNPs decorated with larger proteins such as the fluorescent proteins GFP and mCherry (239 and 236 amino acids, respectively). However, we first analyzed whether TEV-derived VNPs could assemble with GFP or mCherry-fused CPs individually. With this aim, GFP and mCherry cDNAs were cloned fused to the amino terminal end of CP_{TEV}. As previously shown in other works, attempts to present large proteins fused to all the CP subunits frequently lead to defective particle assembly or substantially lower yields. However, this problem can be solved by adding wild-type CP copies to generate mosaic virions. To achieve this, one possibility is to insert the picornavirus F2A ribosome skipping domain to split the linked proteins, resulting in a mix of wild-type and fused proteins.[35] Therefore, in order to anticipate possible limitations on the infectivity of the recombinant TEV clones (TEV/GFP-CP and TEV/mCherry-CP), we also built derivative clones in which the F2A sequence was cloned between the corresponding fluorescent protein and the CP to generate partially decorated VNPs (TEV/GFP-F2A-CP and TEV/mCherry-F2A-CP) (Figure 3A). All recombinant viruses were agroinoculated in *N. benthamiana* plants including TEV-wt and mock-inoculated controls. Pictures of representative upper leaves were taken at 14 dpi (Figure 3B). These images show that symptoms of infection only developed for the F2A-carrying viruses, as well as for the positive wild-type controls, suggesting that the direct fusion of the exogenous proteins interferes with virus replication. In order to confirm that the inserted sequences were still present in the progeny of the recombinant viruses, plant tissues were collected (14 dpi) and the TEV genomes were analyzed via RT-PCR using primers that flanked the insertion site. Amplification products separated via agarose gel electrophoresis showed the presence of bands with the expected position only for the same samples in which symptoms were visually observed (Figure 3C, top). We next analyzed the protein extracts from infected tissues by Western blot with an antibody against CP_{TEV}. Results showed the accumulation of free CP_{TEV} (30 kDa) in plants inoculated with TEV-wt, TEV/GFP-F2A-CP or TEV/mCherry-F2A-CP, while higher bands, likely corresponding to the fluorescent protein-CP_{TEV} fusions (60 kDa), were only seen in plants agroinoculated with TEV/GFP-F2A-CP and TEV/mCherry-F2A-CP (Figure 3C, bottom). In addition to the two expected bands, a third band corresponding to an intermediate size (approximately 42 kDa) was also detected, likely arising from degradation of the larger fused-protein. Hereafter, all virus recombinant clones contained

https://doi.org/10.1021/acsnano.4c07066
ACS Nano 2024, 18, 33890−33906

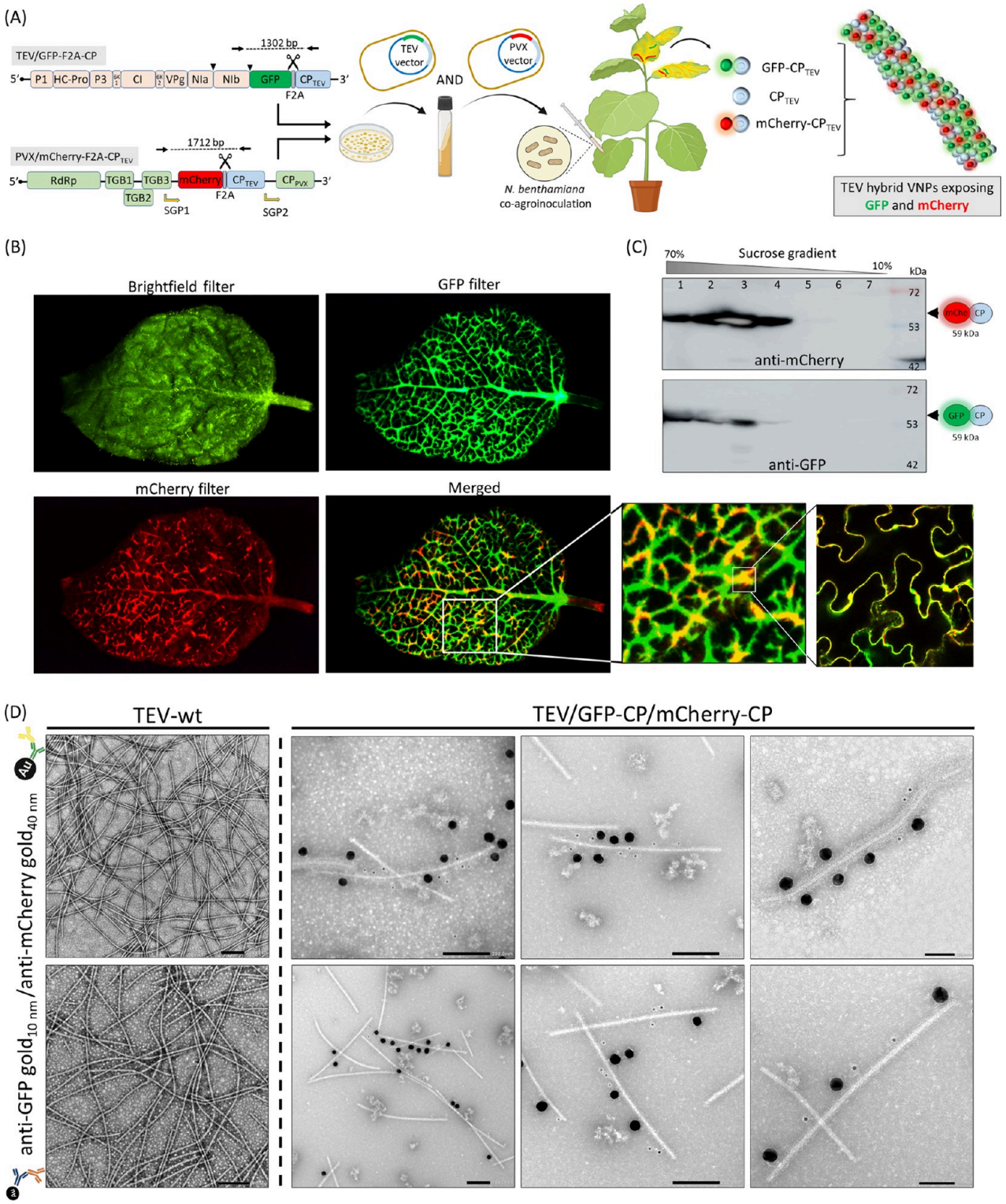

Figure 4. Production of hybrid TEV nanoparticles codecorated with GFP and mCherry. (A) *N. benthamiana* plants were coagroinoculated with the TEV/GFP-F2A-CP and a PVX vector expressing the CP_{TEV} cDNA sequence fused to mCherry (PVX/mCherry-F2A-CP_{TEV}). Cells coinfected with both recombinant viruses express both CP_{TEV}-fused proteins as well as free CP_{TEV} potentially allowing the assembly of hybrid chimeric particles. (B) Representative stereomicroscope pictures of coinfected *N. benthamiana* leaves under visible light, green fluorescence and red fluorescence conditions. The coexpression of GFP and mCherry in the same cells was also confirmed by confocal microscopy. (C) VNPs were purified as previously described. Sucrose gradient fractions were analyzed by Western blot using an antibody against GFP or an antibody against mCherry and positive fractions for both recombinant CPs were pooled, dialyzed, and concentrated. (D) Correct assembly of purified VNPs was observed by TEM negative-staining and the presence of both GFP and mCherry presented on their surface was detected by coimmunostaining with the same antibodies described in Figure 3, except for the anti-rabbit that was conjugated to 40 nm gold spheres. Six different representative images are shown. Images of a TEV-wt negative control are also included on the left.

https://doi.org/10.1021/acsnano.4c07066
ACS Nano 2024, 18, 33890−33906

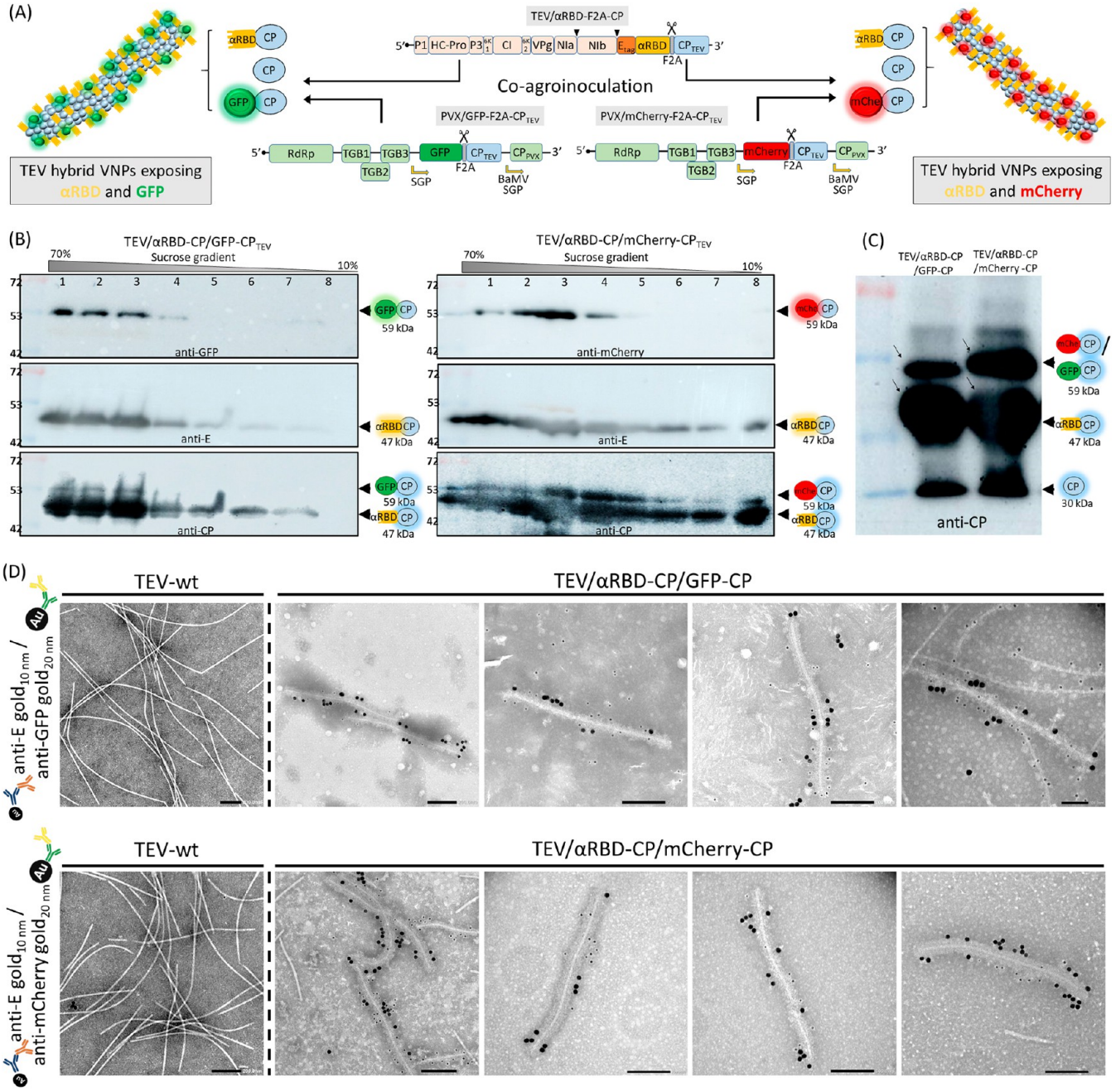

Figure 5. Hybrid VNPs codecorated with a nanobody against SARS-CoV-2 RBD and a fluorescent reporter protein. (A) *N. benthamiana* plants were coagroinoculated with a TEV/αRBD- F2A-CP and a PVX vector expressing the CP_{TEV} cDNA sequence fused to GFP or mCherry. Cells coinfected with both viruses express both CP-fused proteins as well as free CP_{TEV} potentially allowing the assembly of hybrid chimeric particles. (B) Plant symptomatic tissues were collected at 14 dpi, and VNPs were purified as previously described. Sucrose gradient fractions were analyzed by Western blot using the corresponding antibodies (left panel, anti-GFP, anti-E and anti-CP_{TEV}; right panel, anti-mCherry, anti-E and anti-CP_{TEV}). The positions and sizes of protein standards are indicated on the left. Black arrowheads indicate the positions of the respective fused proteins and free CP_{TEV}. (C) Positive fractions for both recombinant CPs were pooled, dialyzed, and concentrated. The purification products were analyzed by Western blot with an anti-CP_{TEV}. (D) Correct assembly of purified VNPs was observed by TEM negative-staining, and the presence of both fused proteins presented on their surface was detected by coimmunostaining. Top, hybrid VNPs presenting αRBD and GFP; αRBD was detected with a primary anti-E and a secondary anti-mouse conjugated to 10 nm gold spheres, while GFP was detected with a primary anti-GFP and a secondary anti-rabbit antibody conjugated to 20 nm gold spheres. Bottom, hybrid VNPs presenting αRBD and mCherry. αRBD was detected with a primary anti-E and a secondary anti-mouse conjugated to 10 nm gold spheres, while mCherry was detected with a primary anti-mCherry and a secondary anti-rabbit antibody conjugated to 20 nm gold spheres. Four different representative images are shown for each hybrid VNP. Images of a TEV-wt negative control immunostaining are shown on the left.

the F2A skipping peptide between the protein of interest and viral CP to produce partially decorated VNPs.

The functionality of the fluorescent proteins was also analyzed by imaging infected *N. benthamiana* leaves with a fluorescence stereomicroscope. Pictures taken under conditions to reveal

https://doi.org/10.1021/acsnano.4c07066
ACS Nano 2024, 18, 33890−33906

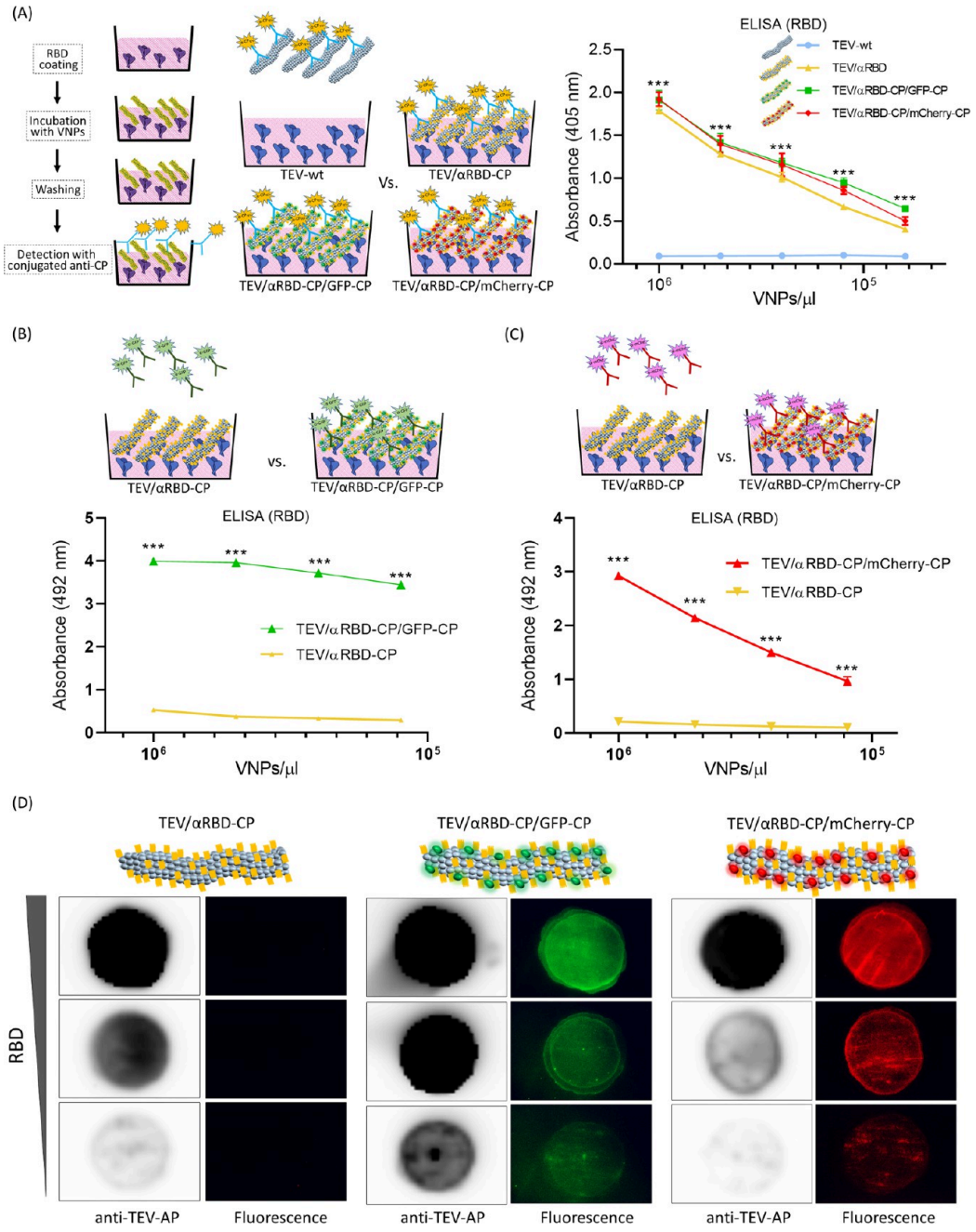

Figure 6. Functionality of hybrid VNPs codecorated with a nanobody against the RBD antigen and a fluorescent reporter protein. (A) Schematic representation of the ELISA to detect RBD. Plates (96-well) were coated with 100 ng/well of recombinant RBD, incubated with serial dilutions of TEV-hybrid VNPs as indicated, extensively washed, and finally revealed using an AP-conjugated anti-CP_{TEV}. TEV-wt and TEV/αRBD-CP VNPs were used as negative and positive control, respectively. Bars represent the means and standard deviations for triplicate samples. Data were analyzed by two-way ANOVA with Tukey's posttest (*, $P < 0.001$). A similar ELISA was performed, but detection was made with an HRP-conjugated anti-GFP (B) or an HRP-conjugated anti-mCherry (C), in both cases using TEV/αRBD-CP VNPs as negative control. (D) Hybrid VNPs functionality was also analyzed by dot-blot assay. Serial dilutions of RBD antigen were coated on a nitrocellulose membrane and incubated with TEV/αRBD-CP, TEV/αRBD-CP/GFP-CP or TEV/αRBD-CP/mCherry-CP VNPs, respectively. Specific interaction was detected with an AP-conjugated anti-CP_{TEV} as positive control and with a stereomicroscope under green and red fluorescence conditions.**

green or red fluorescence showed the expected accumulation of the corresponding fluorescent protein in each case (Figure 3D). VNPs were next purified from infected leaves and analyzed, on the one hand, by Coomassie-stained SDS-PAGE, and on the other hand, by fluorescence imaging of the purified samples under UV light. First analysis showed the presence of both free and fused-CP (Figure 3E, top); second analysis exhibited the expected fluorescence emission (Figure 3E, bottom). Finally, in order to demonstrate that the recombinant fluorescent VNPs were assembled correctly and exposed to the fluorescent proteins on their surface, purified recombinant VNPs were analyzed by IEM. GFP was detected using an anti-GFP and a secondary anti-mouse coupled with gold (10 nm) spheres, while mCherry was detected using an anti-mCherry and a secondary anti-rabbit coupled to gold of 20 nm diameter; a TEV-wt preparation was used as a negative control in both cases. Images

https://doi.org/10.1021/acsnano.4c07066
ACS Nano 2024, 18, 33890−33906

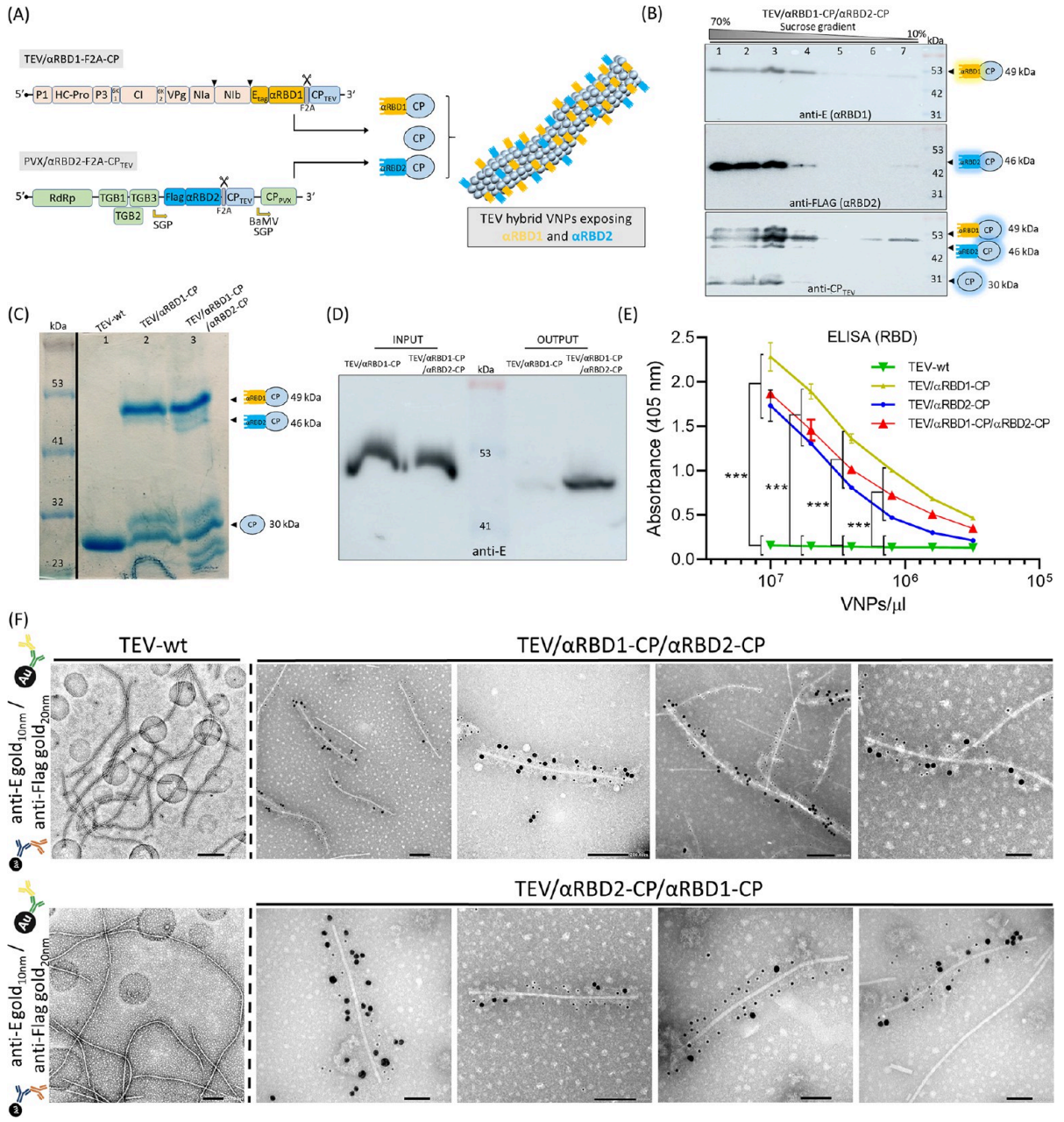

Figure 7. Production of hybrid VNPs codecorated with two nanobodies against different epitopes of RBD. (A) *N. benthamiana* plants were coagroinoculated with a TEV/αRBD1-F2A-CP vector and a PVX vector expressing the CP$_{TEV}$ cDNA sequence fused to αRBD2, which targets a different epitope of RBD. Cells coinfected with both viral vectors express both CP-fused nanobodies as well as free CP$_{TEV}$ potentially allowing the assembling of hybrid chimeric particles. (B) Plant symptomatic tissues were collected at 14 dpi, and VNPs were purified as previously described. Sucrose gradient fractions were analyzed by Western blot using the corresponding antibodies (anti-E for αRBD1-CP, anti-Flag for αRBD2-CP, and anti-CP$_{TEV}$ for all CPs). The positions and sizes of protein standards are indicated on the right. Black arrowheads indicate the positions of the respective fused proteins and free CP$_{TEV}$. (C) Positive fractions for both recombinant CPs were pooled, dialyzed and concentrated. The purification product was analyzed by SDS-PAGE and Coomassie brilliant blue staining (lane 3), including a purified TEV-wt and a purified TEV/αRBD1-CP as references (lanes 1 and 2, respectively). (D) The presence of both fused-CPs in assembled hybrid VNPs was demonstrated by coimmunoprecipitation. Hybrid VNPs were pulled-down with anti-Flag coated agar beads. αRBD1-VNPs were used as a negative control. The co-IP input and output were analyzed by Western blot with an anti-E. (E) An ELISA was performed to detect RBD with the single nanobody expressing VNPs or with the hybrid VNPs. Plates (96-well) were coated with 100 ng/well of recombinant RBD, incubated with serial dilutions of TEV VNPs as indicated, extensively washed, and finally revealed using AP-conjugated anti-CP$_{TEV}$. TEV-wt was used as negative control. Bars represent the means and standard deviations for triplicate samples. Data were analyzed by two-way ANOVA with Tukey's posttest (*, $P < 0.001$). (F) Correct assembly of purified VNPs was observed by TEM negative-staining, and the presence of both fused proteins presented on their surface was detected by coimmunostaining. αRBD1 was detected with a primary anti-E and a secondary anti-mouse conjugated to 10 nm gold particles, while αRBD2 was detected with a primary anti-Flag and a secondary anti-rabbit antibody conjugated to 20 nm gold spheres. Four different representative images are shown for each hybrid VNP. Images of a TEV-wt negative control immunostaining are shown on the left.**

https://doi.org/10.1021/acsnano.4c07066
ACS Nano 2024, 18, 33890−33906

revealed the characteristic TEV filamentous virions specifically decorated with their respective gold spheres (Figure 3F). Taken together, these results demonstrate the feasibility of generating correctly assembled TEV-derived VNPs exposing fluorescent proteins on their surfaces.

Production of Hybrid TEV Nanoparticles Codecorated with GFP and mCherry. To put together the results shown above, we attempted to produce hybrid particles exposing GFP and mCherry in the same recombinant TEV-derived VNP. With this aim, *N. benthamiana* plants were coagroinoculated following the same strategy already described, using the TEV/GFP-F2A-CP and a PVX vector expressing CP_{TEV} fused to mCherry (PVX/mCherry-F2A-CP_{TEV}) (Figure 4A, left side). Cells coinfected with both recombinant viruses should express both CP-fused proteins and free CP_{TEV} potentially allowing the assembling of hybrid chimeric virions (Figure 4A, right side). After 14 days, symptoms were visible in upper leaves of inoculated plants, and both fluorescent proteins accumulated in infected tissues. Representative stereomicroscope pictures of coinfected *N. benthamiana* leaves under white light, and conditions to reveal green and red fluorescence are shown in Figure 4B. GFP and mCherry coexpression in the same cells was also corroborated by confocal microscopy (Figure 4B, merged magnification scheme on the right). Next, VNPs were purified by ultracentrifugation on a sucrose gradient. Both CP-fused fluorescent proteins were observed by Western blot in the same fractions using the correspondent specific antibodies (Figure 4C). Finally, the effective VNP assembly was corroborated by transmission electron microscopy (TEM). The occurrence of both GFP and mCherry presented on their surface was visualized by co-IEM with the specific antibodies described above, except for the anti-rabbit that in this case was conjugated to 40 nm gold spheres, in order to better differentiate sizes (Figure 4D). Images showed the presence of TEV-like particles costained with gold spheres of both sizes, which supported that hybrid VNPs were successfully assembled (TEV/GFP-CP/mCherry-CP). To further support this notion, we also developed the reciprocal coagroinoculation system, using a TEV/mCherry-F2A-CP viral vector and a PVX vector expressing the CP_{TEV} cDNA sequence fused to GFP (PVX/GFP-F2A-CP_{TEV}). Following the same steps previously described, we successfully obtained hybrid particles exposing both fluorescent proteins that were clearly visualized by co-IEM (Supplementary Figure S1).

Hybrid VNPs Codecorated with a Nanobody against SARS-CoV-2 and a Fluorescent Reporter Protein. Next, we considered combining the expression of a nanobody against SARS-CoV-2 RBD (αRBD)[36] with a fluorescent reporter protein on the same hybrid nanoparticle, thus generating a reagent with potential applicability in diagnosis. We coagroinoculated *N. benthamiana* with TEV/αRBD-F2A-CP and a PVX-derivative expressing the CP_{TEV} fused either to GFP or to mCherry (named generically as FP-CP). Of note, the αRBD domain was tagged with an E tag in order to follow its accumulation (Figure 5A). Plant upper symptomatic tissues were collected at the 14 days postion, and VNPs were purified as previously described. We analyzed the sucrose fractions via Western blot using the corresponding antibodies for each fused-CP combination, and positive fractions for both recombinant CPs were pooled, dialyzed and concentrated (Figure 5B). Purified VNPs were analyzed by Western blot with an antibody against the CP_{TEV}. Three main bands were observed that likely correspond to wild-type CP, αRBD-CP and FP-CP (Figure 5C). Purified VNPs were then directly visualized by electron microscopy, and the occurrence of both fused proteins on the exterior was confirmed by co-IEM (Figure 5D). These results indicated that TEV-like virions codecorated with αRBD and GFP or mCherry were successfully assembled.

We next analyzed the functionality of these hybrid VNPs coexhibiting a nanobody against RBD and a fluorescent reporter protein. First, we performed an ELISA against the RBD antigen. Plates (96 wells) were coated with recombinant RBD (100 ng/well). Serial dilutions of hybrid VNPs were used to incubate the plates. After thorough washing, this assay was finally revealed using an alkaline phosphatase (AP)-conjugated anti-CP_{TEV} antibody. We used TEV-wt and TEV/αRBD-CP nanoparticles as negative and positive controls. A schematic representation of the assay is shown in Figure 6A. Both hybrid VNPs produced a signal whose intensity was similar to that produced by the αRBD-decorated TEV positive control. TEV-wt raised no significant signal at any of the concentrations assayed. This result supports the idea that the αRBD nanobody is functional in the context of hybrid VNPs. To demonstrate that these particles were also carrying a fluorescent protein, a similar ELISA against RBD was performed, but binding was indirectly detected through HRP-conjugated anti-GFP (Figure 6B) or HRP-conjugated anti-mCherry (Figure 6C) antibodies. TEV/αRBD-CP was used as a negative control in both cases. These results demonstrate the physical link between αRBD-CP and the FP-CP.

To take advantage of the fluorescent reporter proteins, the functionality of the hybrid VNPs was also monitored by dot-blot assays. For this purpose, serial dilutions of the RBD antigen were spotted on a nitrocellulose membrane, which was incubated with preparations of TEV/αRBD-CP, TEV/αRBD-CP/GFP-CP and TEV/αRBD-CP/mCherry-CP nanoparticles, respectively. Specific interaction was first reveled with an AP-conjugated anti-CP_{TEV} antibody as a positive control and subsequently by visualization using a stereomicroscope under green or red fluorescence conditions, respectively. AP-derived luminescent signals and fluorescent signals correlated and decreased, as expected, with VNP dilutions (Figure 6D). Altogether, these results support the successful generation of functional hybrid VNPs derived from TEV presenting simultaneously a nanobody and fluorescent reporter proteins.

Hybrid VNPs Codecorated with Nanobodies against Different Epitopes of RBD. Finally, we aimed to combine the expression of two different nanobodies on the same hybrid VNP. We envisioned that this kind of polyvalent complex could be equivalent to a nanobody cocktail. In particular, the simultaneous use of antibodies targeting distinct regions of the same viral protein has been proven to be a powerful strategy to overcome the virus mutational scape. Thus, we chose to present two different nanobodies against two distinct epitopes of the RBD antigen that were previously described[36,37] (named here for simplicity, αRBD1 and αRBD2).

Plants were coagroinoculated with TEV/αRBD1-CP, and a recombinant PVX expressing the CP_{TEV} fused to αRBD2 (PVX/αRBD2-F2A-CP_{TEV}). Of note, the αRBD1 domain was tagged with an E tag, while the αRBD2 domain was tagged with a Flag tag, in order to follow their accumulations (Figure 7A). Symptomatic tissues were collected at 14 dpi, and VNPs were purified as previously described. Fractions of the sucrose gradient were analyzed by Western blot with the specific antibodies (anti-E for αRBD1-CP, anti-Flag for αRBD2-CP, and anti-CP_{TEV} to detect all CP forms simultaneously) (Figure 7B).

https://doi.org/10.1021/acsnano.4c07066
ACS Nano 2024, 18, 33890−33906

Fractions with positive signals for both recombinant CPs were pooled, dialyzed, and concentrated. The purified products were visualized by Coomassie staining, including purified TEV-wt and single-decorated αRBD1-VNPs as controls, and next analyzed by Western blot against both fused CPs. Bands of the expected sizes were observed (Figure 7C). The presence of both fused-CPs in assembled hybrid VNPs was evaluated by coimmunoprecipitation. Hybrid VNPs were pulled-down with anti-Flag coated agar beads, and the co-IP inputs and outputs were analyzed by Western blot with an anti-E. Single-decorated αRBD1-VNPs were again used as negative control (Figure 7D). Next, an ELISA was performed to detect RBD with both single nanobody expressing VNPs or with the hybrid VNPs. Plates were coated with recombinant RBD (100 ng/well) and incubated with serial dilutions of VNPs, and the assay was finally revealed using an AP-conjugated anti-CP_{TEV}. TEV-wt was used as negative control. The graph depicting the results showed similar curves for all of the nanobody-carrying VNPs, supporting that hybrid VNPs are equally functional (Figure 7E). In addition, correct assembly of purified hybrid VNPs was observed by co-IEM. αRBD1 was detected using an anti-E followed by a secondary gold-conjugated (10 nm) anti-mouse, while αRBD2 was detected using an anti-Flag and a secondary anti-rabbit coupled to gold (20 nm) (Figure 7F, top line). TEV-like particles decorated with gold spheres of both sizes were successfully observed, confirming the chimeric identity of the VNPs. Finally, an inverted coagroinoculation strategy in which αRBD2 was cloned in the TEV vector and αRBD1-CP_{TEV} in the PVX vector was also performed, and purified VNPs were also analyzed by co-IEM, obtaining similar results (Figure 7F, bottom line).

DISCUSSION

Plant VNPs engineered as scaffolds to expose polypeptides on their surfaces present some outstanding properties. In contrast to most synthetic nanoparticles, they are biocompatible and biodegradable, they self-assemble based on viral CP endogenous properties, and are amenable for inexpensive large-scale production.[4] Moreover, their particulate nature allows the development of easy protocols for purification and concentration. Because plant viruses are not pathogenic to humans and other vertebrates, this kind of VNPs has raised interest in the sector of nanotechnology.[1−4,38,39]

Although initial work in the field was based on icosahedral VNPs,[20] isometric viruses exhibit some limitations for peptide presentation as a consequence of the particle geometry. In contrast, flexuous filamentous viruses provide nanostructures with a higher aspect ratio, increasing the potential sites for functionalization.[23,24] Virions of TEV (genus *Potyvirus*; family *Potyviridae*) are made up of approximately 2000 CP subunits helically arrayed, in which the N-terminal domain is projected toward the external surface of the particle, while the C-terminal end is packaged in the lumen.[40−43] Potyviruses have been already engineered into nanoscaffolds for the presentation of short antigenic peptides exhibiting improved immunogenicity,[26−29] and we previously showed generation of genetically encoded TEV-derived VNPs exposing on their surface nanobodies against different targets.[31,32] Going a step further in this work, we demonstrate the possibility of producing hybrid TEV-derived nanoparticles in *N. benthamiana* biofactory plants. For this, we took advantage of the synergy in mixed infections among PVX and several potyviruses, TEV included.[33,44,45] Both recombinant viruses replicated and spread systemically, reaching the upper leaves, therefore expressing the mixture of modified CPs in the same cells. Co-immunoelectron microscopy assay allows not only to perform a qualitative analysis of VNPs but also to directly visualize antigens and their relative positions within the viral particles.[46] Using this technique, we confirmed that the TEV-derived VNPs assembled properly, forming filamentous particles and, most importantly, that both epitope tags were simultaneously exposed on the outer surface.

Since E and Flag tags are small polypeptides, we explored the replacement of these fused tags with two different fluorescent proteins, GFP and mCherry. We obtained successful results only after using the picornavirus F2A skipping peptide to produce partially decorated VNPs. Production of hybrid plant VNPs displaying two fluorescent proteins as CP fusions was previously reported. Authors used combinations of expression vectors derived from PVX and TMV to produce hybrid PVX nanoparticles.[47] They also performed bimolecular fluorescence complementation (BiFC) assays using a split-mCherry system fused to different PVX CPs to demonstrate hybrid nanoparticles. They found that the direct fusion of these large proteins to the CP impaired particle assembly and thus used the 2A peptide to produce a so-called hybrid overcoat structure on the PVX nanoparticles.[48−50] These results are consistent with several other studies showing that only small polypeptides are able to be expressed linked to the PVX CP N-terminal end, whereas by employing a 2A peptide, VNPs can display larger polypeptides.[49,51−55]

Successful production of decorated VNPs requires careful structural study of the fusion partners, including potential interference on assembly. Some potyviral particles have been structurally analyzed,[41−43] and for turnip mosaic virus (TuMV), the viability of different functionalized VNPs has been studied using advanced computational methodologies that include molecular dynamics.[56,57] These works showed how the high flexibility of the intrinsically disordered region (IDR) comprising the CP N-terminal domain is a key stabilization feature for virion assembly. Attempts to fuse different proteins with variable sizes, structures or interaction energies to this domain resulted in variable results.[6] In this context, the use of a picornavirus F2A skipping peptide contributes to avoid potential disruptive interactions and therefore improves recombinant VNP stability. Moreover, computational analysis has shown the capacity to predict the outcome of recombinant VPNs, which could benefit future work.[57]

Due to their small size and structural simplicity, recombinant VHH or nanobodies are amenable to bioengineering and can be expressed as fusions with other protein domains producing bivalent or multivalent molecules with multispecific binding abilities. Plants hold the potential to produce recombinant antibodies and vaccines to contribute to the global response to pandemics, as recently demonstrated in the case of SARS-CoV-2, based on production speed, scalability, safety, and economic cost.[9,10,13,58−62] We previously developed VNPs presenting single genetically encoded nanobodies against the RBD (Spike protein) of SARS-CoV-2.[32] These nanobodies, originally named VHH-72 and Ty1,[36,37] are here renamed αRBD1 and αRBD2 for simplicity. In this work, we moved forward by producing hybrid TEV-derived VNPs that combine αRBD1 and fluorescent reporter proteins. Both GFP- or mCherry-fused CPs were successfully mix-assembled with αRBD1-fused CPs, as could be shown not only by IEM but also by functional assays in which the interaction of the VNPs with the RBD antigen was

https://doi.org/10.1021/acsnano.4c07066
ACS Nano 2024, 18, 33890−33906

detected by fluorescence analysis. These chimeric VNPs hold promise for use as a diagnostic reagent.

Since the beginning of COVID-19 pandemics, circulating variants of SARS-CoV-2 acquired nucleotide changes that improved viral transmissibility by facilitating escape from immune neutralization.[63−65] Experiments of *in vitro* evolution showed that targeting simultaneously two neutralizing epitopes significantly hinders the emergence of virus escape mutants.[66−68] Multimeric hybrid VNPs displaying several distinct nanobodies may represent powerful escape-resistant therapeutics. Because αRBD1 and αRBD2 do not recognize the same RBD epitope,[69] we considered them proof of this principle by generation of multivalent bispecific VNPs. The functionality of these hybrid VNPs in ELISA was similar to that of the individually decorated VNPs. Future neutralization assays may prove potential increased protection against mutational escape variants.

This work expands the capabilities of plant virus-derived nanoparticles as multifunctional systems. Because of their stability, biocompatibility, and customizable surface functionality, VNPs are considered potential biotechnological tools for therapeutics, diagnostics, and imaging applications. Plant derived VNPs have gained interest in nanomedicine as potential anticancer biomaterials. To circumvent the side effects of some systemic drugs, VNPs are considered for targeted therapeutic approaches with anticancer compounds being directly delivered to tumor cells.[2,70−73] Hybrid VNPs may be engineered with different nanobodies to selectively target cancer cell receptors, increasing the specificity and efficacy of therapeutics.[71] Additionally, plant viruses have been shown to enhance the immunogenicity of peptides through robust presentation to the immune system. Antigen multimeric presentation is a well-established approach to induce strong humoral immune responses.[74] Given that immune responses against single epitopes from pathogens are usually not enough to protect from infection, simultaneous presentation of various epitopes may be a good solution for the development of more effective vaccines.[47] In this line, hybrid VNPs presenting two or more different antigens could widen the range of antibodies induced by recombinant vaccines.[74]

Of course, there are still challenges to overcome. Our results showed that the yields of hybrid VNPs carrying larger proteins were lower than those of VNPs decorated with small tags. Based on the intensity of Coomassie brilliant blue-stained protein bands and comparison with protein standards, yields ranging from 20 to 100 μg per gram (fresh weight) of plant tissue were calculated for the different hybrid VNP preparations. The presence of large fused cargos must limit accumulation of the recombinant viruses when compared to wild-type counterparts. In addition, although the synergistic interaction between PVX and TEV is used here as a platform for the production of hybrid particles, this dual system might also have a negative effect on the yield. The use of two synergic viruses boosts viral accumulation, especially that of PVX, but also increases disease symptoms, with the consequent negative effect on the host plant. It can also be assumed that the number of coinfected cells is only a fraction of those singly infected with one or the other virus. Furthermore, the proportion of functionalized CPs as well as the ratio among cargoes in the hybrid VNPs is expected to change from batch to batch. Future work must definitively focus on optimizing hybrid VNP production. The best ratio among the different *A. tumefaciens* clones or even sequential agroinoculation can be analyzed. Vacuum-based agroinfiltration of the entire plant can also be considered to increase the rate of coinfected cells. Finally, purified VNPs can also be used to infect plants in place of agroinoculation in order to reduce tissue damage or decrease the host response to inoculation.

Despite the production of foreign proteins in plants still exhibis some limitations, not only associated with purification or downstream processing but also with some regulatory issues, many recombinant proteins have been produced with demonstrated safety and efficacy in preclinical and clinical studies.[58] However, for VNP biomedical applications, their interaction with the immune system still requires a deep analysis. In addition, although some methods such as radiation or chemical treatments are expected to produce innocuous nanoparticles, careful evaluation of *in vivo* toxicity and stability is still required.[75]

CONCLUSIONS

In this work, we have reported on the production in *N. benthamiana* plants of genetically encoded plant virus-derived hybrid VNPs, which are used as scaffolds for presenting different nanobodies simultaneously or to combine nanobodies and fluorescent proteins. Potyviruses encompass the largest group of RNA viruses affecting plants, with many species and a collectively wide host range, which will allow exploring different plant species as possible host biofactories. This study contributes to the development of VNPs based on plant viruses as green bionanomaterials that may be useful tools in nanotechnology, particularly in nanomedicine. Sustainably production of biosecure VNPs in plants represents a promising biotechnology with potential to treat a wide variety of diseases affecting humans.

METHODS

Plasmid Construction. Plasmid pGTEVa[76] (Supplementary Figure S2) is a pCLEAN-G181-derivative that contains the cDNA of a TEV sequence variant with GenBank accession number DQ986288, including two silent mutations (G273A, A1119G). In this plasmid, TEV cDNA expression is under the control of the 35S promoter and terminator of cauliflower mosaic virus (CaMV).[77] Plasmid pLBPVX (Supplementary Figure S2) contains a PVX cDNA with GenBank accession number MT799816.1. PVX cDNA is also under the control of the 35S promoter and terminator of CaMV. Starting from pGTEVa and pLBPVX, derivatives were built using common techniques in molecular biology, such as PCR amplification using a high-fidelity DNA polymerase (Phusion; Thermo Scientific), DNA cleavage using restriction enzymes and DNA joining[78] with the NEBuilder HiFi DNA assembly master mix (New England Biolabs). To prepare TEV recombinant clones, exogenous cDNAs were inserted at the 5′ side of CP_{TEV} gene, with or without the picornavirus F2A peptide[35] in between. The three first codons of CP_{TEV}, although with silent mutations, were repeated to facilitate proteolytic cleavage mediated by viral NIaPro. To prepare PVX recombinant clones, the exogenous cDNAs were inserted as an independent ORF after the CP_{PVX} promoter. In these clones, PVX CP contains a deletion of the 29 codons at the N-terminal end and is expressed through a heterologous promoter derived from a related potexvirus, bamboo mosaic virus (BaMV).[79] Sequences of all TEV and PVX recombinant clones are in Supplementary Figures S3 and S4, respectively.

Inoculation of Plants. *N. benthamiana* was cultivated at 25 °C in growth chambers with a 16/8 h light/darkness cycle. Plasmids containing TEV recombinant clones were used to transform the C58C1 strain of *A. tumefaciens*. In this case, the strain also contained pCLEAN-S48 as a helper plasmid.[77] After electroporation, *A. tumefaciens* were grown in the presence of 50, 50, and 7.5 μg/mL of kanamycin, rifampicin, and tetracycline, respectively. In the case of recombinant PVX clones, the *A. tumefaciens* C58C1 strain was used

https://doi.org/10.1021/acsnano.4c07066
ACS Nano 2024, 18, 33890−33906

with no helper plasmid. After electroporation, *A. tumefaciens* were grown in plates containing only 50 μg/mL of each kanamycin and rifampicin. Selected colonies were grown in liquid media for 24 h at 28 °C to reach 0.5 to 1 optical density at 600 nm (OD_{600}). Bacteria were centrifuged and resuspended at OD_{600} of 0.5 in agroinoculation medium[32] (10 mM MES-NaOH [pH 5.6], 10 mM $MgCl_2$, and 150 μM acetosyringone). The preparation was subjected to induction for 2 h (28 °C). *N. benthamiana* plants (4−6 weeks old) were infiltrated in fully expanded upper leaves with *A. tumefaciens* cultures harboring PVX or TEV clones using a needleless syringe. After infiltration, *N. benthamiana* plants were grown at 25 °C under a cycle of 16/8-h light/darkness. At 14 dpi, in general, tissues with symptoms were harvested from apical leaves, as well as similar tissues from controls mock-inoculated. Tissues were stored frozen at −80 °C.

Analysis of the Viral Progeny via RT-PCR. Leaf tissue aliquots were treated to purify the RNA with silica columns (Zymo Research). In the case of PVX analysis, RNA preparations were retrotranscribed with RevertAid reverse transcriptase (Thermo Scientific) and oligodeoxynucleotide 5′-CTCTTTAATTGCTGCTGC-3′. RT reaction was followed by PCR amplification using oligodeoxynucleotides 5′-GCCATTGCCGATCTCAAGCCAC-3′ and 5′-GCTACTATGGCACGGGCTGTAC-3′, which flanked the N-terminal end of CP_{PVX}. In the case of TEV, cDNA synthesis was performed with oligodeoxynucleotide 5′-TCATAACCCAAGTTCCGTTC-3′. DNA amplification was carried out using oligodesoxynucleotides 5′-CATCTGTGCATCAATGATCGAA-3′ and 5′-GTGTGGCTCGAGCATTTGACAA-3′, which flanked the N-terminal end of CP_{TEV}. PCR amplification products were electrophoresed in agarose gels (1%; w/v). Gels were finally soaked in 1% (w/v) ethidium bromide for 15 min for staining.

Western-Blot Analysis. Frozen tissues (aliquots of about 50 mg) were ground (Star-Beater, VWR) with a steel ball (4 mm) for 1 min at a frequency of 30 s^{-1} in protein extraction buffer[32] (60 mM Tris-HCl [pH 6.8], 2% [w/v] SDS, 100 mM dithiothreitol [DTT], 10% [v/v] glycerol, 0.01% [w/v] bromophenol blue) which was added at a 3:1 ratio. After thorough vortexing, samples were incubated (100 °C) for 5 min and subjected to centrifugation for 5 min. SDS-PAGE using 12% (w/v) polyacrylamide gel was employed to separate the aliquots of the supernatants. Proteins were next electroblotted for 1 h to polyvinylidene difluoride (PVDF) membranes. Membranes were first subjected to blocking for 1 h in washing buffer[32] (10 mM Tris-HCl [pH 7.5], 154 mM NaCl, 0.1% [w/v] Nonidet P-40) containing 5% (w/v) nonfat milk. Membranes were next incubated at 4 °C overnight in blocking solution with the corresponding antibodies at 1:10,000 dilutions. Detection of CP_{TEV} was done with a polyclonal antibody (Agdia), which was coupled to AP. Detection of epitopes E and Flag as well as GFP was done with monoclonal antibodies (Thermo Scientific) coupled to HRP. mCherry was detected with a specific antibody (Abcam) followed by a secondary HRP-conjugated antirabbit. Membranes were washed three times with washing buffer between primary and secondary antibodies prior to detection. AP and HRP were revealed using CSPD (Roche) and SuperSignal West Pico PLUS chemiluminescent (Thermo Scientific) substrates, respectively. An Amersham ImageQuant 800 (Cytiva) instrument was used to record the images.

Viral Particle Purification. A Polytron (Kinematica) was used to grind symptomatic leaf tissue with two volumes of homogenization buffer[32] (50 mM sodium phosphate, 10 mM EDTA, 10% ethanol, pH 7.2). After the homogenate was filtered through Miracloth (Millipore) and centrifuged (7800 rpm, 20 min) for clarification, the supernatant was incubated for 1 h in the presence of 10 mM 2-mercaptoethanol and 1% Triton X-100, and subjected again to centrifugation for 20 min at 7800 rpm. After recovering the supernatant, ultracentrifugation was used to sediment VNPs for 2 h at 130 000*g* and 4 °C. Sediments containing VNPs were resuspended in a volume of 1 mL in buffer 50 mM sodium phosphate and 1% Triton X-100. Preparations were layered on a 10% to 70% sucrose gradient (10 mL). After centrifugation (130 000*g*, 4 °C) for 3 h, fractions (1 mL) were recovered and VNPs were analyzed by Western blot. Those fractions containing VNPs were combined and subjected to dialysis against a phosphate-buffered saline (PBS) solution. Preparations were finally concentrated using Centricon 100 kDa filters (Millipore) and stored at 4 °C.

Quantification of Viral Particles. SDS-PAGE was used to separate purified samples; gels were stained with Coomassie brilliant blue. A standard curve was obtained using bovine serum albumin (BSA) to evaluate the VNP amount using ImageJ. Additionally, quantification of the number of copies of viral genomes was performed by RT-quantitative PCR (qPCR). To this purpose, VNPs were first denatured by heating at 98 °C for 5 min, and the viral RNA was subjected to cDNA synthesis (see above). To perform qPCR, the iTaq Universal SYBR Green Supermix (Bio-Rad) was used in combination with olidodeoxynucleotides 5′-AGTGGCACTGTGGGTGCTGGTGTTG-3′ and 5′-GTGTGGCTCGAGCATTTGACAA-3′ flanking the CP_{TEV} N-terminal region.

Immunogold Electron Microscopy Staining. First, VNPs (15-μL aliquots) were adsorbed on carbon film-coated 200 mesh copper grids (EMS) at room temperature during 15 min. Grids were then blocked with 15 μL of 1% BSA in PBS. Grids were subsequently subjected to incubation with 15 μL of one or more of the previously described antibodies during 2 h (1:50 dilution in blocking buffer). The grids were subjected to washing twice with PBS and incubation continued during 1 h with gold-conjugated secondary antibody (10 μL). Grids were washed twice with PBS followed by 4 additional washing steps of 1 min with H_2O. Grids were stained with 10 μL of 2% (w/v) phosphotungstic acid (PTA; pH 7.0) and dried at room temperature for 3 min. Finally, a JEM-1400Flash (120 kV) electron microscope (JEOL) was used to analyze the preparations.

Pull-down Assays. The interaction of different fused-CPs was evaluated by coimmunoprecipitation assays using anti-DYKDDDDK tag affinity beads (Abcam) which bind to the Flag sequence, following the instructions provided by the manufacturer. Affinity beads were completely resuspended, and a 40 μL suspension was added to a 1.5 mL Eppendorf tube. After centrifugation for 30 s at 5000*g*, the sediment was resuspended with binding buffer (500 μL). This step was repeated twice. Before the VNPs sample was added to the tube, they were centrifuged for 60 s at 5000*g* in order to avoid the sedimentation of unspecific pre-existing aggregates. Clarified VNPs (200 μL) were added to the resuspended affinity beads, mixed by gently inverting the tube, and kept with mixing on a rotator for 2 h. The mixture was centrifuged for 30 s at 5000*g*. The sediment was then resuspended in 500 μL of wash buffer by mixing on a rotator for 10 min. The mixture was centrifuged again in the same conditions as above, discarding the supernatant. This step was repeated three times, making sure that all supernatant was finally removed. Finally, elution was performed by adding 20 μL of 2X SDS-PAGE loading buffer to the tube, mixing well, and heating at 100 °C for 5 min. After centrifugation for 30 s at 5000*g*, the supernatant was recovered and analyzed by Western blot using the corresponding antibodies.

ELISA. RBD detection using VNPs were done as previously described.[32] Briefly, 96 well plates were loaded with 100 ng/well of recombinant RBD (Thermo Scientific, RP-87678) in coating buffer (15 mM Na_2CO_3, 35 mM $NaHCO_3$, pH 9.8). After washing plates twice with 300 μL of PBS containing 0.1% (v/v) Tween-20 (300 μL/well) and blocking for 2 h with 200 μL of blocking solution (5% nonfat milk in PBS-T; 200 μL/well) at room temperature, an incubation with 1:5 serial dilutions of VNPs in blocking solution was performed for 2 h. Dilutions in a total of 100 μL/well started at 10^6 VNPs/μL per well (100 μL). Plates were next washed four times with PBS-T, incubated in blocking solution containing an AP-conjugated anti-CP_{TEV} and washed again four times. Finally, after incubation with 100 μL of *para*-nitrophenyl phosphate (pNPP, 1 mg/mL), a multiwell plate reader (TECAN) was employed to measure (405 nm) absorbance. For detecting GFP and mCherry, a similar protocol was performed, but incubating with an antibody conjugated to HRP, and using the *o*-phenylenediamine dihydrochloride (OPD) as substrate (Sigma-Aldrich), following manufacturer instructions. In this case, absorbance (492 nm) was measured with a multiwell plate reader.

Dot Blot Analysis. RBD serial dilutions were directly spotted in 10 μL drops onto a nitrocellulose membrane. Drops were allowed to dry for 10 min. A blocking step was performed during 1 h in the presence of

https://doi.org/10.1021/acsnano.4c07066
ACS Nano 2024, 18, 33890−33906

5% (w/v) nonfat milk in washing buffer (see above). Membranes were incubated next with recombinant VNPs. After washing, VNP binding was detected directly using a fluorescence stereomicroscope or indirectly by incubating with an AP-conjugated anti-CP_{TEV} antibody followed by incubation with the corresponding substrate, as previously described.

ASSOCIATED CONTENT

Supporting Information

The Supporting Information is available free of charge at https://pubs.acs.org/doi/10.1021/acsnano.4c07066.

Production of hybrid TEV nanoparticles codecorated with GFP and mCherry using an inverted vector combination. Nucleotide sequences of plasmids used in this work. Nucleotide sequences of all the recombinant TEV and PVX derived clones used in this work. (PDF)

AUTHOR INFORMATION

Corresponding Authors

José-Antonio Daròs − *Instituto de Biología Molecular y Celular de Plantas (Consejo Superior de Investigaciones Científicas − Universitat Politècnica de València), 46022 Valencia, Spain*; orcid.org/0000-0002-6535-2889; Email: jadaros@ibmcp.upv.es

Fernando Merwaiss − *Instituto de Biología Molecular y Celular de Plantas (Consejo Superior de Investigaciones Científicas − Universitat Politècnica de València), 46022 Valencia, Spain*; Email: fmerwaiss@upv.es

Author

Enrique Lozano-Sanchez − *Instituto de Biología Molecular y Celular de Plantas (Consejo Superior de Investigaciones Científicas − Universitat Politècnica de València), 46022 Valencia, Spain*

Complete contact information is available at: https://pubs.acs.org/10.1021/acsnano.4c07066

Author Contributions

The work was conceived by J.-A.D. and F.M. with contribution from E.L.S. The experiments were performed by E.L.S. and F.M.. Data analysis was performed by all authors. The manuscript was written by J.-A.D. and F.M. with contribution from E.L.-S. All authors discussed, revised and approved the manuscript.

Notes

The authors declare no competing financial interest.

ACKNOWLEDGMENTS

Ministerio de Ciencia, Innovación y Universidades through Agencia Estatal de Investigación (MICIU/AEI; Spain) supported this research through grants PID2020-114691RB-I00, MICIU/AEI/10.13039/501100011033; and PLEC2022-009400, MICIU/AEI/10.13039/501100011033 and NextGenerationEU/PRTR. Generalitat Valenciana also supported this research through grant PROMETEO CIPROM/2022/21. F.M. is the recipient of a postdoctoral contract (CIAPOS/2021/277) from Generalitat Valenciana. E.L.-S. is the recipient of a predoctoral contract (PRE2021-097401) from MICIU.

REFERENCES

(1) Rybicki, E. P. Plant Molecular Farming of Virus-like Nanoparticles as Vaccines and Reagents. *WIREs Nanomed Nanobiotechnol* **2020**, *12*, e1587.

(2) Chung, Y. H.; Cai, H.; Steinmetz, N. F. Viral Nanoparticles for Drug Delivery, Imaging, Immunotherapy, and Theranostic Applications. *Adv. Drug Delivery Rev.* **2020**, *156*, 214−235.

(3) Venkataraman, S.; Hefferon, K. Application of Plant Viruses in Biotechnology, Medicine, and Human Health. *Viruses* **2021**, *13*, 1697.

(4) Dickmeis, C.; Kauth, L.; Commandeur, U. From Infection to Healing: The Use of Plant Viruses in Bioactive Hydrogels. *WIREs Nanomed Nanobiotechnol* **2021**, *13*, e1662.

(5) Porta, C.; Lomonossoff, G. P. Scope for Using Plant Viruses to Present Epitopes from Animal Pathogens. *Rev. Med. Virol.* **1998**, *8* (1), 25−41.

(6) Röder, J.; Dickmeis, C.; Commandeur, U. Small, Smaller, Nano: New Applications for Potato Virus X in Nanotechnology. *Front. Plant Sci.* **2019**, *10* (February), 1−17.

(7) Yuste-Calvo, C.; González-Gamboa, I.; Pacios, L. F.; Sánchez, F.; Ponz, F. Structure-Based Multifunctionalization of Flexuous Elongated Viral Nanoparticles. *ACS Omega* **2019**, *4* (3), 5019−5028.

(8) Fischer, R.; Buyel, J. F. Molecular Farming - The Slope of Enlightenment. *Biotechnol. Adv.* **2020**, *40*, 107519.

(9) Schillberg, S.; Finnern, R. Plant Molecular Farming for the Production of Valuable Proteins - Critical Evaluation of Achievements and Future Challenges. *J. Plant Physiol.* **2021**, *258*−*259*, 153359.

(10) Lobato Gómez, M.; Huang, X.; Alvarez, D.; He, W.; Baysal, C.; Zhu, C.; Armario-Najera, V.; Blanco Perera, A.; Cerda Bennasser, P.; Saba-Mayoral, A.; Sobrino-Mengual, G.; Vargheese, A.; Abranches, R.; Abreu, I. A.; Balamurugan, S.; Bock, R.; Buyel, J. F.; da Cunha, N. B.; Daniell, H.; Faller, R.; Folgado, A.; Gowtham, I.; Häkkinen, S. T.; Kumar, S.; Ramalingam, S. K.; Lacorte, C.; Lomonossoff, G. P.; Luís, I. M.; Ma, J. K. C.; McDonald, K. A.; Murad, A.; Nandi, S.; O'Keefe, B.; Oksman-Caldentey, K. M.; Parthiban, S.; Paul, M. J.; Ponndorf, D.; Rech, E.; Rodrigues, J. C. M.; Ruf, S.; Schillberg, S.; Schwestka, J.; Shah, P. S.; Singh, R.; Stoger, E.; Twyman, R. M.; Varghese, I. P.; Vianna, G. R.; Webster, G.; Wilbers, R. H. P.; Capell, T.; Christou, P. Contributions of the International Plant Science Community to the Fight against Human Infectious Diseases - Part 1: Epidemic and Pandemic Diseases. *Plant Biotechnol. J.* **2021**, *19* (10), 1901−1920.

(11) Benvenuto, E.; Broer, I.; D'Aoust, M. A.; Hitzeroth, I.; Hundleby, P.; Menassa, R.; Oksman-Caldentey, K. M.; Peyret, H.; Salgueiro, S.; Saxena, P.; Stander, J.; Warzecha, H.; Ma, J. Plant Molecular Farming in the Wake of the Closure of Medicago Inc. *Nat. Biotechnol.* **2023**, *41* (7), 893−894.

(12) Tschofen, M.; Knopp, D.; Hood, E.; Stöger, E. Plant Molecular Farming: Much More than Medicines. *Annu. Rev. Anal. Chem.* **2016**, *9*, 271−294.

(13) Tusé, D.; Nandi, S.; Mcdonald, K. A.; Buyel, J. F. The Emergency Response Capacity of Plant-Based Biopharmaceutical Manufacturing-What It Is and What It Could Be. *Front. Plant Sci.* **2020**, *11*, 594019.

(14) Hefferon, K. Plant Virus Expression Vectors: A Powerhouse for Global Health. *Biomedicines* **2017**, *5*, 44.

(15) Narayanan, K. B.; Han, S. S. Recombinant Helical Plant Virus-Based Nanoparticles for Vaccination and Immunotherapy. *Virus Genes* **2018**, *54* (5), 623−637.

(16) Chung, Y. H.; Church, D.; Koellhoffer, E. C.; Steinmetz, N. F. Integrating Plant Molecular Farming and Materials Research for Next-Generation Vaccines. *Nat. Rev. Mater.* **2022**, *7*, 372−388.

(17) Chung, Y. H.; Ortega-Rivera, O. A.; Volckaert, B. A.; Jung, E.; Zhao, Z.; Steinmetz, N. F. Viral Nanoparticle Vaccines against S100A9 Reduce Lung Tumor Seeding and Metastasis. *Proc. Natl. Acad. Sci. U. S. A.* **2023**, *120* (43), e2221859120.

(18) Beatty, P. H.; Lewis, J. D. Cowpea Mosaic Virus Nanoparticles for Cancer Imaging and Therapy. *Adv. Drug Delivery Rev.* **2019**, *145*, 130−144.

(19) Ortega-Rivera, O. A.; Shukla, S.; Shin, M. D.; Chen, A.; Beiss, V.; Moreno-Gonzalez, M. A.; Zheng, Y.; Clark, A. E.; Carlin, A. F.; Pokorski, J. K.; Steinmetz, N. F. Cowpea Mosaic Virus Nanoparticle Vaccine Candidates Displaying Peptide Epitopes Can Neutralize the Severe Acute Respiratory Syndrome Coronavirus. *ACS Infect. Dis.* **2021**, *7* (11), 3096−3110.

(20) Sainsbury, F.; Cañizares, M. C.; Lomonossoff, G. P. Cowpea Mosaic Virus: The Plant Virus-Based Biotechnology Workhorse. *Annu. Rev. Phytopathol.* **2010**, *48*, 437−455.
(21) Lomonossoff, G. P.; Wege, C. TMV Particles: The Journey From Fundamental Studies to Bionanotechnology Applications. *Adv. Virus Res.* **2018**, *102*, 149−175.
(22) Röder, J.; Fischer, R.; Commandeur, U.; Schiemann, J. H.; Kühninstitut, J. Adoption of the 2A Ribosomal Skip Principle to Tobacco Mosaic Virus for Peptide Display. *Front. Plant Sci.* **2017**, *8*, 1125.
(23) Shukla, S.; Ablack, A. L.; Wen, A. M.; Lee, K. L.; Lewis, J. D.; Steinmetz, N. F. Increased Tumor Homing and Tissue Penetration of the Filamentous Plant Viral Nanoparticle Potato Virus X. *Mol. Pharmaceutics* **2013**, *10* (1), 33−42.
(24) Lagarrigue, P.; Moncalvo, F.; Cellesi, F. Non-Spherical Polymeric Nanocarriers for Therapeutics: The Effect of Shape on Biological Systems and Drug Delivery Properties. *Pharmaceutics* **2023**, *15*, 32.
(25) Kapate, N.; Clegg, J. R.; Mitragotri, S. Non-Spherical Micro- and Nanoparticles for Drug Delivery: Progress over 15 Years. *Adv. Drug Delivery Rev.* **2021**, *177*, 113807.
(26) Fernández-Fernández, M. R.; Martínez-Torrecuadrada, J. L.; Roncal, F.; Domínguez, E.; García, J. A. Identification of Immunogenic Hot Spots within Plum Pox Potyvirus Capsid Protein for Efficient Antigen Presentation. *J. Virol.* **2002**, *76* (24), 12646−12653.
(27) Yuste-Calvo, C.; López-Santalla, M.; Zurita, L.; Cruz-Fernández, C. F.; Sánchez, F.; Garín, M. I.; Ponz, F. Elongated Flexuous Plant Virus-Derived Nanoparticles Functionalized for Autoantibody Detection. *Nanomaterials* **2019**, *9*, 1438.
(28) Manuel-cabrera, C. A.; Vallejo-cardona, A. A.; Padilla-camberos, E.; Hernández-gutiérrez, R.; Herrera-rodríguez, S. E.; Gutiérrez-ortega, A. Self-Assembly of Hexahistidine-Tagged Tobacco Etch Virus Capsid Protein into Microfilaments That Induce IgG2-Specific Response against a Soluble Porcine Reproductive and Respiratory Syndrome Virus Chimeric Protein. *Virol. J.* **2016**, *13*, 1−6.
(29) González-Gamboa, I.; Manrique, P.; Sánchez, F.; Ponz, F. Plant-Made Potyvirus-like Particles Used for Log-Increasing Antibody Sensing Capacity. *J. Biotechnol.* **2017**, *254*, 17−24.
(30) Martínez-Turiño, S.; García, J. A. Potyviral Coat Protein and Genomic RNA: A Striking Partnership Leading Virion Assembly and More. *Adv. Virus Res.* **2020**, *108*, 165−211.
(31) Martí, M.; Merwaiss, F.; Butković, A.; Daròs, J. A. Production of Potyvirus-Derived Nanoparticles Decorated with a Nanobody in Biofactory Plants. *Front. Bioeng. Biotechnol.* **2022**, *10*, 877363.
(32) Merwaiss, F.; Lozano-Sanchez, E.; Zulaica, J.; Rusu, L.; Vazquez-Vilar, M.; Orzáez, D.; Rodrigo, G.; Geller, R.; Daròs, J. A. Plant Virus-Derived Nanoparticles Decorated with Genetically Encoded SARS-CoV-2 Nanobodies Display Enhanced Neutralizing Activity. *Plant Biotechnol. J.* **2024**, *22*, 876−891.
(33) Wang, Y.; Gaba, V.; Yang, J.; Palukaitis, P.; Gal-On, A. Characterization of Synergy between Cucumber Mosaic Virus and Potyviruses in Cucurbit Hosts. *Phytopathology* **2002**, *92* (1), 51−58.
(34) De, S.; Chavez-Calvillo, G.; Wahlsten, M.; Mäkinen, K. Disruption of the Methionine Cycle and Reduced Cellular Gluthathione Levels Underlie Potex-Potyvirus Synergism in Nicotiana Benthamiana. *Mol. Plant Pathol.* **2018**, *19* (8), 1820−1835.
(35) Kim, J. H.; Lee, S. R.; Li, L. H.; Park, H. J.; Park, J. H.; Lee, K. Y.; Kim, M. K.; Shin, B. A.; Choi, S. Y. High Cleavage Efficiency of a 2A Peptide Derived from Porcine Teschovirus-1 in Human Cell Lines, Zebrafish and Mice. *PLoS One* **2011**, *6* (4), e18556.
(36) Wrapp, D.; De Vlieger, D.; Corbett, K. S.; Torres, G. M.; Wang, N.; Van breedam, W.; McLellan, J. S. Structural Basis for Potent Neutralization of Betacoronaviruses by Single-Domain Camelid Antibodies. *Cell* **2020**, *181*, 1004−1015.
(37) Hanke, L.; Perez, L. V.; Sheward, D. J.; Das, H.; Schulte, T.; Moliner-morro, A.; Corcoran, M.; Achour, A.; Hedestam, G. B. K.; Hällberg, B. M.; Murrell, B.; Mcinerney, G. M. An Alpaca Nanobody Neutralizes SARS-CoV-2 by Blocking Receptor Interaction. *Nat. Commun.* **2020**, *11*, 4420.
(38) Marsian, J.; Lomonossoff, G. P. Molecular Pharming-VLPs Made in Plants. *Curr. Opin. Biotechnol.* **2016**, *37*, 201−206.
(39) Eiben, S.; Koch, C.; Altintoprak, K.; Southan, A.; Tovar, G.; Laschat, S.; Weiss, I. M.; Wege, C. Plant Virus-Based Materials for Biomedical Applications: Trends and Prospects. *Adv. Drug Delivery Rev.* **2019**, *145*, 96−118.
(40) Kavčič, L.; Kežar, A.; Koritnik, N.; Žnidarič, M. T.; Klobučar, T.; Vičič, Ž.; Merzel, F.; Holden, E.; Benesch, J. L. P.; Podobnik, M. From Structural Polymorphism to Structural Metamorphosis of the Coat Protein of Flexuous Filamentous Potato Virus Y. *Commun. Chem.* **2024**, *7*, 14.
(41) Zamora, M.; Mendez-Lopez, E.; Agirrezabala, X.; Cuesta, R.; Lavin, J. L.; Sanchez-Pina, M. A.; Aranda, M. A.; Valle, M. Potyvirus Virion Structure Shows Conserved Protein Fold and RNA Binding Site in SsRNA Viruses. *Sci. Adv.* **2017**, *3*, eaao218220.
(42) Cuesta, R.; Yuste-calvo, C.; Gil-cartón, D.; Sánchez, F.; Ponz, F.; Valle, M. Structure of Turnip Mosaic Virus and Its Viral-like Particles. *Sci. Rep.* 2019, *9*, 15396. .
(43) Kežar, A.; Kavčič, L.; Polák, M.; Nováček, J.; Gutiérrez-Aguirre, I.; Žnidarič, M. T.; Coll, A.; Stare, K.; Gruden, K.; Ravnikar, M.; Pahovnik, D.; Žagar, E.; Merzel, F.; Anderluh, G.; Podobnik, M. Structural Basis for the Multitasking Nature of the Potato Virus Y Coat Protein. *Sci. Adv.* **2019**, *5*, eaaw3808.
(44) Mascia, T.; Gallitelli, D. Synergies and Antagonisms in Virus Interactions. *Plant Sci.* **2016**, *252*, 176−192.
(45) Pruss, G.; Ge, X.; Shi, X. M.; Carrington, J. C.; Vance, V. B. Plant Viral Synergism: The Potyviral Genome Encodes a Broad-Range Pathogenicity Enhancer That Transactivates Replication of Heterologous Viruses. *Plant Cell* **1997**, *9* (6), 859−868.
(46) Gulati, N. M.; Torian, U.; Gallagher, J. R.; Harris, A. K. Immunoelectron Microscopy of Viral Antigens. *Curr. Protoc. Microbiol.* **2019**, *53*, e86.
(47) Dickmeis, C.; Honickel, M. M. A.; Fischer, R.; Commandeur, U. Production of Hybrid Chimeric PVX Particles Using a Combination of TMV and PVX-Based Expression Vectors. *Front. Bioeng. Biotechnol.* **2015**, *3*, 189.
(48) Smolenska, L.; Roberts, I. M.; Learmonth, D.; Porter, A. J.; Harris, W. J.; Wilson, T. M. A.; Santa Cruz, S. Production of a Functional Single Chain Antibody Attached to the Surface of a Plant Virus. *FEBS Lett.* **1998**, *441* (3), 379−382.
(49) Cruz, S S; Chapman, S; Roberts, A G; Roberts, I M; Prior, D A; Oparka, K J Assembly and Movement of a Plant Virus Carrying a Green Fluorescent Protein Overcoat. *Proc. Natl. Acad. Sci. U. S. A.* **1996**, *93*, 6286−6290.
(50) Castells-Graells, R.; Lomonossoff, G. P.; Saunders, K. Production of Mosaic Turnip Crinkle Virus-like Particles Derived by Coinfiltration of Wild-Type and Modified Forms of Virus Coat Protein in Plants. *Methods Mol. Biol.* **2018**, *1776*, 3−17.
(51) Marconi, G.; Albertini, E.; Barone, P.; De Marchis, F.; Lico, C.; Marusic, C.; Rutili, D.; Veronesi, F.; Porceddu, A. In Planta Production of Two Peptides of the Classical Swine Fever Virus (CSFV) E2 Glycoprotein Fused to the Coat Protein of Potato Virus X. *BMC Biotechnol.* **2006**, *6*, 29.
(52) Röder, J.; Dickmeis, C.; Fischer, R.; Commandeur, U. Systemic Infection of Nicotiana Benthamiana with Potato Virus X Nanoparticles Presenting a Fluorescent ILOV Polypeptide Fused Directly to the Coat Protein. *Biomed Res. Int.* **2018**, *2018*, 9328671.
(53) Shukla, S.; Dickmeis, C.; Nagarajan, A. S.; Fischer, R.; Commandeur, U.; Steinmetz, N. F. Molecular Farming of Fluorescent Virus-Based Nanoparticles for Optical Imaging in Plants, Human Cells and Mouse Models. *Biomater. Sci.* **2014**, *2* (5), 784−797.
(54) Shukla, S.; Dickmeis, C.; Fischer, R.; Commandeur, U.; Steinmetz, N. F. In Planta Production of Fluorescent Filamentous Plant Virus-Based Nanoparticles. *Methods Mol. Biol.* **2018**, *1776*, 61−84.
(55) Uhde-Holzem, K.; Schlösser, V.; Viazov, S.; Fischer, R.; Commandeur, U. Immunogenic Properties of Chimeric Potato Virus X Particles Displaying the Hepatitis C Virus Hypervariable Region I Peptide R9. *J. Virol. Methods* **2010**, *166*, 12−20.
(56) Mínguez-Toral, M.; Pacios, L. F.; Sánchez, F.; Ponz, F. Structural Intrinsic Disorder in a Functionalized Potyviral Coat Protein as a Main

https://doi.org/10.1021/acsnano.4c07066
ACS Nano 2024, 18, 33890−33906

Viability Determinant of Its Assembled Nanoparticles. *Int. J. Biol. Macromol.* **2023**, *236*, 123958.
(57) Pacios, L. F.; Sánchez, F.; Ponz, F. Intrinsic Disorder in the Dynamic Evolution of Structure, Stability, and Flexibility of Potyviral VLP Assemblies: A Computational Study. *Int. J. Biol. Macromol.* **2024**, *254*, 127798.
(58) Donini, M.; Marusic, C. Current State-of-the-Art in Plant-Based Antibody Production Systems. *Biotechnol. Lett.* **2019**, *41* (3), 335−346.
(59) Diamos, A. G.; Hunter, J. G. L.; Pardhe, M. D.; Rosenthal, S. H.; Sun, H.; Foster, B. C.; DiPalma, M. P.; Chen, Q.; Mason, H. S. High Level Production of Monoclonal Antibodies Using an Optimized Plant Expression System. *Front. Bioeng. Biotechnol.* **2020**, *7*, 472.
(60) Swope, K.; Morton, J.; Pogue, G. P.; Burden, L.; Partain, N.; Hume, S.; Shepherd, J.; Simpson, C. A.; Brennan, M. B.; Furman, T. C.; Kingrey-Gebe, S.; Martinez, T.; McDonough, J.; Pauly, M. H.; Whaley, K. J.; Zeitlin, L.; Bratcher, B.; Haydon, H. Reproducibility and Flexibility of Monoclonal Antibody Production with Nicotiana Benthamiana. *MAbs* **2022**, *14* (1), e2013594.
(61) Lico, C.; Santi, L.; Baschieri, S.; Noris, E.; Marusic, C.; Donini, M.; Pedrazzini, E.; Maga, G.; Franconi, R.; Di Bonito, P.; Avesani, L. Plant Molecular Farming as a Strategy Against COVID-19 - The Italian Perspective. *Front. Plant Sci.* **2020**, *11*, 609910.
(62) Capell, T.; Twyman, R. M.; Armario-Najera, V.; Ma, J. K. C.; Schillberg, S.; Christou, P. Potential Applications of Plant Biotechnology against SARS-CoV-2. *Trends Plant Sci.* **2020**, *25* (7), 635−643.
(63) Casasnovas, J. M.; Margolles, Y.; Noriega, M. A.; Guzmán, M.; Arranz, R.; Melero, R.; Casanova, M.; Corbera, J. A.; Jiménez-de-Oya, N.; Gastaminza, P.; Garaigorta, U.; Saiz, J. C.; Martín-Acebes, M. Á.; Fernández, L. Á. Nanobodies Protecting From Lethal SARS-CoV-2 Infection Target Receptor Binding Epitopes Preserved in Virus Variants Other Than Omicron. *Front. Immunol.* **2022**, *13*, 863831.
(64) Harvey, W. T.; Carabelli, A. M.; Jackson, B.; Gupta, R. K.; Thomson, E. C.; Harrison, E. M.; Ludden, C.; Reeve, R.; Rambaut, A.; Peacock, S. J.; Robertson, D. L. SARS-CoV-2 Variants, Spike Mutations and Immune Escape. *Nat. Rev. Microbiol.* **2021**, *19* (7), 409−424.
(65) Chen, R. E.; Zhang, X.; Case, J. B.; Winkler, E. S.; Liu, Y.; VanBlargan, L. A.; Liu, J.; Errico, J. M.; Xie, X.; Suryadevara, N.; Gilchuk, P.; Zost, S. J.; Tahan, S.; Droit, L.; Turner, J. S.; Kim, W.; Schmitz, A. J.; Thapa, M.; Wang, D.; Boon, A. C. M.; Presti, R. M.; O'Halloran, J. A.; Kim, A. H. J.; Deepak, P.; Pinto, D.; Fremont, D. H.; Crowe, J. E.; Corti, D.; Virgin, H. W.; Ellebedy, A. H.; Shi, P. Y.; Diamond, M. S. Resistance of SARS-CoV-2 Variants to Neutralization by Monoclonal and Serum-Derived Polyclonal Antibodies. *Nat. Med.* **2021**, *27* (4), 717−726.
(66) Koenig, P. A.; Das, H.; Liu, H.; Kümmerer, B. M.; Gohr, F. N.; Jenster, L. M.; Schiffelers, L. D. J.; Tesfamariam, Y. M.; Uchima, M.; Wuerth, J. D.; Gatterdam, K.; Ruetalo, N.; Christensen, M. H.; Fandrey, C. I.; Normann, S.; Tödtmann, J. M. P.; Pritzl, S.; Hanke, L.; Boos, J.; Yuan, M.; Zhu, X.; Schmid-Burgk, J. L.; Kato, H.; Schindler, M.; Wilson, I. A.; Geyer, M.; Ludwig, K. U.; Hällberg, B. M.; Wu, N. C.; Schmidt, F. I. Structure-Guided Multivalent Nanobodies Block SARS-CoV-2 Infection and Suppress Mutational Escape. *Science.* **2021**, *371*, 691.
(67) Xiang, Y.; Nambulli, S.; Xiao, Z.; Liu, H.; Sang, Z.; Duprex, W. P.; Schneidman-Duhovny, D.; Zhang, C.; Shi, Y. Versatile and Multivalent Nanobodies Efficiently Neutralize SARS-CoV-2. *Science.* **2020**, *370*, 1479−1484.
(68) Mast, F. D.; Fridy, P. C.; Ketaren, N. E.; Wang, J.; Jacobs, E. Y.; Olivier, J. P.; Sanyal, T.; Molloy, K. R.; Schmidt, F.; Rutkowska, M.; Weisblum, Y.; Rich, L. M.; Vanderwall, E. R.; Dambrauskas, N.; Vigdorovich, V.; Keegan, S.; Jiler, J. B.; Stein, M. E.; Olinares, P. D. B.; Herlands, L.; Hatziioannou, T.; Sather, D. N.; Debley, J. S.; Fenyö, D.; Sali, A.; Bieniasz, P. D.; Aitchison, J. D.; Chait, B. T.; Rout, M. P. Highly Synergistic Combinations of Nanobodies That Target SARS-CoV-2 and Are Resistant to Escape. *Elife* **2021**, *10*, e73027.
(69) Jin, D.; Wei, J.; Sun, J. Analysis of the Molecular Mechanism of SARS-CoV-2 Antibodies. *Biochem. Biophys. Res. Commun.* **2021**, *566*, 45−52.
(70) Thuenemann, E. C.; Le, D. H. T.; Lomonossoff, G. P.; Steinmetz, N. F. Bluetongue Virus Particles as Nanoreactors for Enzyme Delivery and Cancer Therapy. *Mol. Pharmaceutics* **2021**, *18* (3), 1150−1156.
(71) Shahgolzari, M.; Venkataraman, S.; Osano, A.; Akpa, P. A.; Hefferon, K. Plant Virus Nanoparticles Combat Cancer. *Vaccines* **2023**, *11* (8), 1278.
(72) Shukla, S.; Roe, A. J.; Liu, R.; Veliz, F. A.; Commandeur, U.; Wald, D. N.; Steinmetz, N. F. Affinity of Plant Viral Nanoparticle Potato Virus X (PVX) towards Malignant B Cells Enables Cancer Drug Delivery. *Biomater. Sci.* **2020**, *8* (14), 3935−3943.
(73) Truchado, D. A.; Juárez-Molina, M.; Rincón, S.; Zurita, L.; Tomé-Amat, J.; Lorz, C.; Ponz, F. A Multifunctionalized Potyvirus-Derived Nanoparticle That Targets and Internalizes into Cancer Cells. *Int. J. Mol. Sci.* **2024**, *25*, 4327.
(74) Brinkkemper, M.; Veth, T. S.; Brouwer, P. J. M.; Turner, H.; Poniman, M.; Burger, J. A.; Bouhuijs, J. H.; Olijhoek, W.; Bontjer, I.; Snitselaar, J. L.; Caniels, T. G.; van der Linden, C. A.; Ravichandran, R.; Villaudy, J.; van der Velden, Y. U.; Sliepen, K.; van Gils, M. J.; Ward, A. B.; King, N. P.; Heck, A. J. R.; Sanders, R. W. Co-Display of Diverse Spike Proteins on Nanoparticles Broadens Sarbecovirus Neutralizing Antibody Responses. *iScience* **2022**, *25* (12), 105649.
(75) Ma, Y.; Steinmetz, N. F. Potato Virus X Inactivation and Characterization. *Methods Mol. Biol.* **2023**, *2671*, 257−271.
(76) Bedoya, L. C.; Martínez, F.; Orzáez, D.; Daròs, J. A. Visual Tracking of Plant Virus Infection and Movement Using a Reporter MYB Transcription Factor That Activates Anthocyanin Biosynthesis. *Plant Physiol.* **2012**, *158* (3), 1130−1138.
(77) Thole, V.; Worland, B.; Snape, J. W.; Vain, P. The PCLEAN Dual Binary Vector System for Agrobacterium-Mediated Plant Transformation. *Plant Physiol.* **2007**, *145*, 1211−1219.
(78) Gibson, D. G.; Young, L.; Chuang, R.-Y. Y.; Venter, J. C.; Hutchison III, C. A.; Smith, H. O. Enzymatic Assembly of DNA Molecules up to Several Hundred Kilobases. *Nat. Methods* **2009**, *6* (5), 343−345.
(79) Dickmeis, C.; Fischer, R.; Commandeur, U. Potato Virus X-Based Expression Vectors Are Stabilized for Long-Term Production of Proteins and Larger Inserts. *Biotechnol. J.* **2014**, *9* (11), 1369−1379.

https://doi.org/10.1021/acsnano.4c07066
ACS Nano 2024, 18, 33890−33906